Constraints on ultralight bosons from merging binary and remnant black holes observed during the second and third parts of the fourth LIGO-Virgo-KAGRA observing run

A. G. Abac *et al.*[*]
(LIGO Scientific Collaboration, Virgo Collaboration, and KAGRA Collaboration)

(Received 11 August 2026; accepted 30 September 2026; published 12 November 2026)

We present constraints on ultralight bosons using binary black hole mergers observed in the second and third parts of the fourth LIGO-Virgo-KAGRA observing run. Directed searches are conducted for long-transient gravitational waves from ultralight vector boson clouds around merger remnants, using a hidden-Markov-model (HMM) tracking scheme. We target the remnant black holes formed in the binary coalescences that produced GW250114 and GW250207. We find no evidence for such signals from either target. Estimating our search sensitivity at a threshold corresponding to a 1% false alarm probability, we thus disfavor vector boson masses in the range of $[2.80, 3.95] \times 10^{-13}$ eV with greater than 90% confidence. In addition, we derive constraints on ultralight scalar and vector bosons from the inferred high spins of the constituent black holes in three binaries, using events GW240515, GW241113, and GW241225_08. The excluded mass ranges in this approach depend on the assumed black-hole ages. At 10^5 years, corresponding to typical dynamically formed binaries, we exclude scalar and vector bosons in the ranges $[1.39, 6.94] \times 10^{-13}$ eV and $[0.32, 14.4] \times 10^{-13}$ eV at 90% confidence, respectively.

DOI: 10.1103/dgjv-chmt

I. INTRODUCTION

Ultralight bosons arise in a variety of extensions of the Standard Model and can provide viable dark matter candidates [1–4]. Motivated examples include axionlike particles and other spin-0 fields [5,6], as well as hidden-sector vector (spin-1) bosons such as dark photons [7–12]. Even if these particles interact only through gravity, rotating black holes can trigger superradiant instabilities that populate bound states of the bosonic field. The resulting boson clouds can grow to macroscopic occupation numbers and act as long-lived sources of nearly monochromatic gravitational radiation, potentially observable with ground-based detectors [13–30].

A rotating black hole becomes superradiantly unstable to an ultralight bosonic field of mass m_b when the condition

$$\omega_b < m\Omega_H \tag{1}$$

is satisfied. Here, $\omega_b \approx m_b c^2/\hbar$ is the angular frequency of the bosonic field, m is the azimuthal quantum number of the bosonic bound state, and Ω_H is the angular frequency of the black hole horizon. The instability is most efficient when the boson Compton wavelength λ is comparable to the black hole gravitational radius r_g, causing the occupation number of the bound state to grow exponentially. The instability extracts energy and angular momentum from the black hole into the bosonic field, leading to a coupled evolution in which the black hole spins down while the cloud grows. If gravitational interactions dominate, this process results in the amplification of the field into a macroscopic boson cloud, which can extract up to ∼10% of the initial black hole mass [13,27,28,31–36].

This extraction continues until the superradiance condition in Eq. (1) begins to saturate ($\omega_b \approx m\Omega_H$), at which point the black hole has spun down sufficiently to shut off the instability. When it satisfies the superradiant condition, the $m = 1$ mode is typically the fastest growing and most relevant for a newly formed black hole. Even after the saturation of this mode, higher modes can continue to grow through superradiance and further spin down the black hole. The boson cloud then depletes through gravitational-wave emission at approximately twice the oscillation frequency, with a small positive frequency drift as the binding energy decreases [20,27–29,37–40]. For stellar- and intermediate-mass black holes and boson masses in the range $\sim 10^{-14} - 10^{-11}$ eV [16,19], this emission falls within the sensitive band of ground-based gravitational-wave detectors. Current and future detector networks [41–46] therefore provide a promising avenue to probe ultralight bosons. In addition,

[*]Full author list given at the end of the article.

Published by the American Physical Society under the terms of the Creative Commons Attribution 4.0 International license. Further distribution of this work must maintain attribution to the author(s) and the published article's title, journal citation, and DOI.

measurements of black hole spins offer a complementary probe, as superradiance-induced spin-down can imprint observable signatures on the spin distribution of merging systems [13,16,19,22,28].

Constraints on ultralight scalar [16,19,22,47–52] and vector [20,22,48,50] bosons have been derived using black hole spin measurements, although these are limited by uncertainties in inferred spins and masses arising from modelling assumptions and observational systematics [53–55]. Searches for continuous gravitational waves, including all-sky and Galactic-center targeted analyses, also constrain scalar bosons under assumptions about the black hole population (mass, spin, and age distributions), disfavoring masses of order $\sim 10^{-13} - 10^{-12}$ eV [56–61]. Similarly, stochastic background searches for populations of black holes with scalar [61–63] and vector [64] clouds disfavor boson masses around $\sim 10^{-13}$ eV, subject to population modelling assumptions. Directed searches targeting Cygnus X-1 exclude scalar and vector bosons in the range $\sim [0.6, 1] \times 10^{-12}$ eV and $\sim [0.9, 1.6] \times 10^{-13}$ eV, respectively, depending on the assumed black hole age and initial spin [65–67]. A continuous-wave search targeting pulsar-catalog sources as candidate luminous dark-photon clouds constrained kinetically mixed dark photons under assumptions about the black hole population and electromagnetic emission [68]. While these results overlap with the parameter space considered in this work, they rely on astrophysical assumptions regarding black hole populations, evolution, and ages; as such, their implications for ultralight bosons in these ranges should be interpreted with caution. In addition to indirect searches, ground-based interferometers have been used for direct searches for ultralight scalars [69–72] and vectors [72–74]. Future observations may also probe the impact of boson clouds on binary black hole inspirals for certain masses and field strengths [23,75–78].

In this study, we present results from two complementary approaches to probe ultralight bosons with gravitational-wave observations. First, we perform a directed search for long-duration transient gravitational-wave signals (on a timescale of hours to months) from vector boson clouds around merger-remnant black holes using a hidden Markov model (HMM) [79,80]. Targeting newly formed black holes with well-characterized properties enables robust constraints with reduced reliance on assumptions about the underlying black hole population and age. Although scalar boson clouds around merger remnant black holes can also generate long-duration gravitational waves [37,81], their strain amplitudes are generally expected to lie below the sensitivity of current-generation detectors. Vector boson clouds, by contrast, are expected to produce stronger and shorter-lived emission, making them more favorable targets for directed searches with current-generation detectors [79]. This approach follows Refs. [79,80] and was previously applied to O4a events [67], constituting the first directed gravitational-wave search for ultralight vector bosons targeting merger remnants. In O4a, the merger remnants of GW230814_230901 and GW231123_135430 (hereafter GW230814 and GW231123) were targeted, yielding weakly disfavored vector boson masses of $[0.94, 1.08] \times 10^{-13}$ eV and $[2.75, 3.28] \times 10^{-13}$ eV at ∼30% confidence. Reference [67] also performed a continuous-wave search using the band sampled data framework, targeting an older galactic black hole in Cygnus X-1 and excluding vector boson masses in the range $[0.85, 1.59] \times 10^{-13}$ eV at 95% confidence, assuming an initial black hole spin $\gtrsim 0.5$. In this work, we extend the HMM analysis to two especially well-suited events from the second and third parts of the fourth LVK observing run (O4b [82] and O4c [83]), focusing on merger remnants formed in binary black hole coalescences. For the remnant search targeting the early post-merger epoch, we consider only the fastest-growing mode with azimuthal number $m = 1$. This study demonstrates that directed searches targeting these events can already strongly disfavor vector boson masses within a relatively narrow mass range set by the remnant properties.

Second, we derive constraints from pre-merger black hole spin measurements following Ref. [48]. This approach identifies regions of parameter space incompatible with efficient superradiant spin-down, thereby constraining the allowed boson masses. In this spin-based analysis, we consider all relevant azimuthal modes that can grow within the assumed black-hole lifetime. Previous studies have shown that events such as GW190517_055101, GW231123, and GW241110_124123 disfavor scalar and vector bosons over the mass ranges $[0.55, 26] \times 10^{-13}$ eV and $[0.11, 53] \times 10^{-13}$ eV, respectively, at a 90% confidence level, assuming black hole lifetimes $\gtrsim 10^5$ yr [48,50]. We extend this analysis to high-spin events observed during O4b and reported in GWTC-5 [82,84,85], providing a complementary and relatively model-independent probe of ultralight bosons.

The paper is organized as follows. In Sec. II, we identify the target sources used in both analyses. In Sec. III, we present the HMM-based search for long-duration transient gravitational-wave signals from ultralight vector boson clouds, including the search methodology, configuration, candidate follow-up procedure, and the resulting disfavored parameter space. In Sec. IV, we describe the complementary analysis based on black hole spin measurements, outlining the method and presenting the corresponding results. Finally, we summarize our findings in Sec. V.

II. TARGET SOURCES

In this section, we describe the black hole systems targeted by the two complementary analyses presented in this work and summarize the gravitational-wave and superradiance parameters relevant to each.

TABLE I. Properties of the merger remnants targeted in the HMM search.

Source [a,b]	M_i $[M_\odot]$	χ_i	D_L [Mpc]	$\cos\iota$	90% credible sky area [deg^2]
GW250114	$62.7^{+1.0}_{-1.1}$	$0.68^{+0.01}_{-0.01}$	403^{+74}_{-70}	$0.64^{+0.18}_{-1.4}$	254.01
GW250207	$62.8^{+0.9}_{-1.4}$	$0.69^{+0.01}_{-0.01}$	188^{+118}_{-52}	$0.38^{+0.30}_{-0.1}$	18.46

[a]We use M_i and χ_i to denote the mass and dimensionless spin of the black hole before superradiance occurs, corresponding to the final black hole mass M_f and spin χ_f inferred from the compact-binary-coalescence PE. We avoid using M_f and χ_f here to prevent confusion with the black hole mass and spin after superradiance.

[b]The two remnant black holes have similar masses and spins; however, differences in detector duty cycles and data quality lead to complementary results from these two targets (see Sec. III).

A. Merger remnant black holes

The merger remnants analyzed in this work are selected based on their expected detectability under the ultralight vector boson cloud scenario. For a subset of compact binary coalescence candidates with a high signal-to-noise ratio (SNR) identified in O4b and O4c, we use the median estimated source properties from GWTC-5 for O4b and from the preliminary parameter-estimation (PE) results available at the time for O4c [82,83,85–90]. For each event, we estimate the maximum detectable luminosity distance, referred to as the horizon distance, for boson-cloud gravitational-wave emission from a black hole with the corresponding median remnant mass and spin, and compare it with the median estimated luminosity distance D_L.[1] The horizon distances are estimated empirically through simulations over the remnant mass and spin parameter space, as described in Ref. [79]. Systems with D_L smaller than the horizon distance are expected to lie within the sensitivity reach of the HMM search. Two merger remnants satisfy this criterion with high confidence in the preliminary selection: GW250114_082203 in O4b and GW250207_115645 in O4c (hereafter GW250114 and GW250207), among the loudest gravitational-wave signals observed to date [82]. Using the final PE results [83,89,90], we verify that the luminosity distances of both systems lie well within their corresponding horizon distances. The estimated horizon distances are approximately 574 Mpc for GW250114 and 592 Mpc for GW250207, substantially larger than their median luminosity distances of 403 Mpc and 188 Mpc, respectively.

The median parameters for each remnant and the 90% credible sky area are summarized in Table I, where M and χ denote the mass and dimensionless spin of the black hole prior to superradiance, D_L is the luminosity distance, and ι is the inclination angle. The sky localizations for both events are shown in Fig. 1. Although the two events have different localization uncertainties, both localizations are sufficiently compact for the search considered here (see relevant search configuration in Sec. III C). The PE results used for GW250114 and GW250207 are obtained with the NRSur7dq4 waveform model [91]. This model is employed because it interpolates directly between numerical relativity simulations within its training domain, thereby reducing additional waveform-modeling assumptions, and is among the most reliable waveform models for relatively heavy binary black hole systems and their remnant properties.

B. Premerger black holes with high spin

In addition to merger remnants, we target compact binary coalescences exhibiting highly spinning constituent black holes prior to merger. The presence of large dimensionless spins provides a complementary probe of ultralight bosons through black hole superradiance: if a boson with a given mass exists, rapidly rotating black holes are expected to spin down over astrophysical timescales. Therefore, the observation of high spins can be used to exclude regions of the boson mass parameter space.

Events considered in this analysis are selected based on (i) evidence for high constituent spins and (ii) well-constrained spin posteriors. Specifically, we require that the median effective inspiral spin satisfies $|\chi_{\rm eff}| > 0.2$, and that at least one component black hole has a median dimensionless spin magnitude greater than 0.5, with its 5th percentile exceeding 0.3. The additional requirement on the 5th percentile ensures that the inferred high spin is not driven solely by the posterior median, and disfavors systems whose posterior distributions retain substantial support for low spins. Applying these criteria to the O4b catalog (reported in GWTC-5 [82]) yields three events of particular interest: GW240515_005301, GW241113_163507, and GW241225_082815 (hereafter GW240515, GW241113, and GW241225_08[2]).

We use PE results obtained with the BILBY framework [92,93] and the DYNESTY sampler [94], employing the NRSur7dq4 waveform model [91] for GW240515 and

[1]Here, the horizon distance refers to the reach for gravitational-wave emission from the vector-boson cloud around the remnant black hole, rather than for the binary merger itself. The evaluation using median values is intended only as a representative criterion for target selection. The selection is deliberately permissive rather than strict, since the horizon distance is, by definition, an optimistic estimate of the detectable reach.

[2]We define the longer abbreviated name GW241225_08 for GW241225_082815 because GWTC-5 contains two events from 2024 December 25.

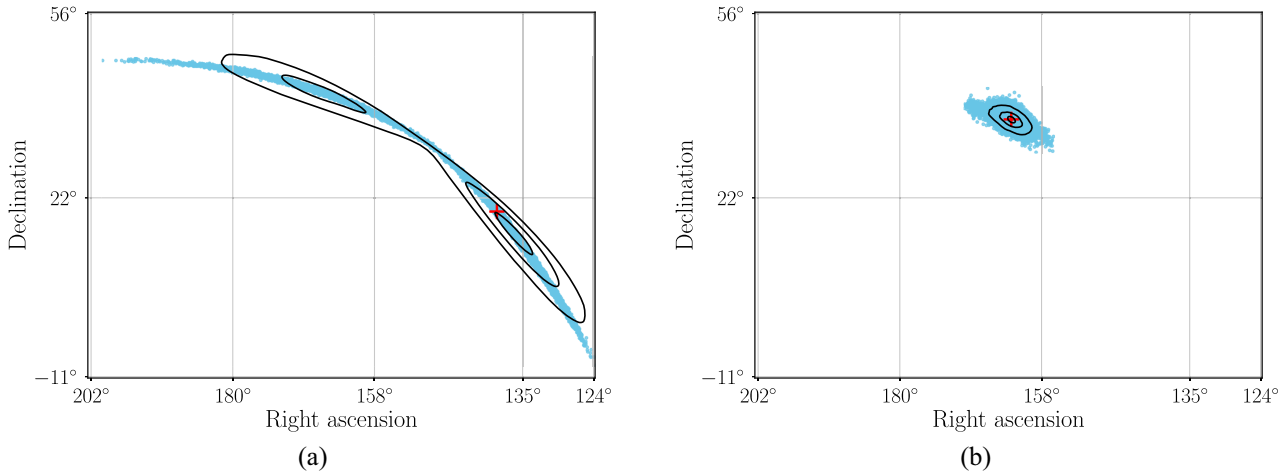


FIG. 1. Joint right ascension and declination posterior distribution for GW250114 (a) and GW250207 (b). The blue points represent sky-position samples from the full posterior distribution. The black contours show the 90%, 50%, and 10% credible intervals. The plus markers indicate the sky positions targeted in the search for each remnant black hole (median values of the distributions).

GW241225_08 and the IMRPhenomXPHM-SpinTaylor waveform model [95,96] for GW241113.[3] NRSur7dq4 was trained on numerical-relativity simulations with component spin magnitudes $\chi_{1,2} \leq 0.8$ [91]. It has also been used in parameter-estimation analyses allowing larger spins, which require extrapolation beyond the training domain [82,97]. For events with posterior support above this threshold, particularly GW241225_08, this extrapolation represents a potential source of waveform-model uncertainty in the inferred spins and resulting superradiance constraints. From these PE results, we extract the primary and secondary masses (m_1, m_2), the corresponding dimensionless spin magnitudes (χ_1, χ_2), the luminosity distance D_{L}, and the network SNR. The median values of these parameters are summarized in Table II.

III. SEARCHES TARGETING MERGER REMNANTS

A. Method

The directed searches are performed using the HMM tracking pipeline described in Refs. [79,80] and applied previously in O4a [67]. Although the signal evolution is well modeled for fixed source parameters, the parameter space in boson mass and remnant black-hole properties is too large for a fully coherent matched-filter search over signal durations ranging from hours to months. The HMM approach therefore provides a computationally tractable way to track the expected frequency evolution while maintaining good coverage of the relevant parameter space.

[3]NRSur7dq4 is used where applicable because it provides reliable parameter estimates for systems in the higher-mass range [91]. For the lower-mass event GW241113, which lies outside the NRSur7dq4 coverage, we instead use IMRPhenomXPHM-SpinTaylor [95,96].

The pipeline computes a coherent multidetector $\mathcal{F}$ statistic [98–100] by coherently combining short Fourier transforms over segments of duration T_{coh}, referred to as the coherent integration time. The HMM then tracks the signal frequency evolution across segments via the Viterbi algorithm [101], without requiring phase coherence between segments. Longer T_{coh} improves sensitivity when the signal remains well matched to the coherent template, but also narrows the frequency bins. Rapid frequency evolution therefore limits the coherent integration time, as excessive drift within a segment spreads the signal power across multiple bins and reduces sensitivity. We choose T_{coh} (and corresponding frequency resolution) based on the maximum expected frequency derivative of the signal, ensuring that the signal remains approximately monochromatic within each segment and evolves by at most one frequency bin between adjacent segments. The significance of candidate tracks is quantified using a log-likelihood-based detection statistic $\mathcal{L}$, normalized by the number of segments N_T as $\bar{\mathcal{L}} \equiv \mathcal{L}/N_T$, allowing for consistent comparison across different search configurations. We refer the reader to Refs. [67,79,80] for a detailed description of the pipeline and its implementation. For the synthetic-signal simulations in this study, we compute vector-boson signal waveforms using the superradiance waveform model SuperRad [40,102], and generate the simulated data with the simulateCW module of the LALPulsar package in LALSuite [103,104].

As the remnant black holes are relatively young and isolated, the corresponding signals are expected to last hours to months and can exhibit rapid frequency evolution. We therefore employ the HMM search method, which is well-suited to signals with significant frequency drift and associated uncertainties.

TABLE II. Median source parameters of the high-spin premerger systems selected from O4b.

Source	m_1 $[M_\odot]$	m_2 $[M_\odot]$	χ_1	χ_2	D_L [Mpc]	SNR
GW240515	$36.8^{+11.6}_{-10.1}$	$18.5^{+8.7}_{-4.5}$	$0.71^{+0.25}_{-0.38}$	$0.56^{+0.39}_{-0.50}$	$3794^{+1840.21}_{-1876.50}$	$10^{+1.7}_{-1.7}$
GW241113	$19.3^{+5.4}_{-3}$	$14.3^{+2.7}_{-3.3}$	$0.80^{+0.17}_{-0.38}$	$0.56^{+0.39}_{-0.49}$	$1355.44^{+666.50}_{-631.87}$	$11.7^{+1.7}_{-1.7}$
GW241225_08	$58.5^{+11.1}_{-9.9}$	$36.3^{+9.7}_{-11.1}$	$0.84^{+0.14}_{-0.41}$	$0.48^{+0.46}_{-0.43}$	$1972^{+1166.74}_{-954.62}$	$17.7^{+1.7}_{-1.6}$

B. Signal parameter space

We specialize to vector bosons and denote their mass by m_V. Using the SuperRad waveform model [40,102] together with the median black hole mass and spin estimates listed in Table I, we determine the optimal boson mass $m_V^{\rm opt}$ that maximizes the superradiant instability for the corresponding black hole. This $m_V^{\rm opt}$ corresponds to the vector-boson mass for which the gravitational-wave strain amplitude is maximized at the reference time $t_{\rm ref}$, when the $m = 1$ mode reaches saturation. For GW250114 and GW250207, we evaluate the representative boson masses $m_V^{\rm opt} = 3.5 \times 10^{-13}$ and 3.6×10^{-13} eV, respectively, corresponding to the median remnant black hole parameters (see Table III). Using these values $m_V^{\rm opt}$ and the median remnant black hole parameters, we compute the corresponding gravitational-wave signal properties during the early postmerger epoch with the SuperRad model, assuming the dominant $m = 1$ superradiant mode. The resulting signal parameters, listed in Table III, are defined as follows. The detector-frame growth and depletion timescales, $\tau^{\rm det}_{\rm growth}$ and $\tau^{\rm det}_{\rm GW}$, describe the evolution of the boson cloud. The former is the inverse growth rate, while the latter corresponds to the gravitational-wave emission timescale. The quantities $h_0^{\rm eff}$, f_0, and $\dot{f}_0$ denote the effective strain, detector-frame signal frequency, and frequency drift at $t_{\rm ref}$. The effective strain amplitude seen by the detector is given by $h_0^{\rm eff} = h_0 2^{-1/2}\{[(1+\cos^2\iota)/2]^2 + \cos^2\iota\}^{1/2}$ [105], where h_0 is the gravitational-wave strain on Earth from a source at luminosity distance D_L, and ι is the inclination angle.[4] The detailed signal evolution model is described in Appendix A. The signal properties evaluated at $m_V^{\rm opt}$ with the median remnant parameters in Table III provide representative examples of the expected signals for the two targets. The search itself is not restricted to these values: it covers a range of vector boson masses and accounts for uncertainties in the remnant black hole properties through their posterior distributions (see Sec. III C).

[4]Here, we use ι, the angle between the binary orbital angular momentum and the line of sight, instead of the viewing angle θ_{JN}, defined as the angle between the total angular momentum of the binary and the line of sight. For GW250114 and GW250207, the posterior distributions of these two angles are similar because both systems have nearly equal component masses, small component spins, and no evidence for significant spin precession.

We consider a search mass range of $[0.6, 1.1]m_V^{\rm opt}$, over which the method is expected to be sensitive, as determined empirically in Ref. [80]. This corresponds to $[2.13, 3.90] \times 10^{-13}$ eV for GW250114 and $[2.18, 3.99] \times 10^{-13}$ eV for GW250207. The range includes vector masses that, while having lower strain amplitude, can yield longer-lived gravitational-wave emission, allowing longer coherent integration times and, in some cases, greater sensitivity than at $m_V^{\rm opt}$.

C. Dataset and search configuration

In this section, we describe the dataset and analysis setup used to perform a directed search for long-transient gravitational-wave emission from the merger remnants of GW250114 and GW250207.

We analyze calibrated, analysis-ready strain data from the Advanced LIGO detectors [41] at Hanford (H1) and Livingston (L1) during the O4b and O4c observing period [106–110]. The strain is produced by the low-latency calibration pipeline (C00), with gating applied to suppress transient noise artifacts and improve the robustness of the HMM search [111]. We use the gated strain channels `H1:GDS-CALIB_STRAIN_CLEAN_GATED_G02` and `L1:GDS-CALIB_STRAIN_CLEAN_GATED_G02` [107,111–118].

Within the vector-boson mass search ranges of $[2.13, 3.90] \times 10^{-13}$ eV for GW250114 and $[2.18, 3.99] \times 10^{-13}$ eV for GW250207, each boson mass maps to a distinct gravitational-wave emission frequency, corresponding to detector-frame frequency ranges of [92, 175] and [96, 185] Hz, respectively. We divide these ranges into 1 Hz subbands over which the search is performed. Given the relatively precise sky localization of these sources (see Table I), we adopt the median right ascension and declination shown in Fig. 1 as fixed sky positions for the search. Although nearly monochromatic, the targeted signals are

TABLE III. Estimated gravitational-wave signal parameters (at the reference time) for the merger remnant targets using the median black hole parameters and their respective $m_V^{\rm opt}$ values.

Source	$m_V^{\rm opt}$ $[10^{-13}$ eV]	$\tau_{\rm growth}$ [h]	$\tau_{\rm GW}$ [h]	$h_0^{\rm eff}$ $[10^{-24}]$	f_0 [Hz]	$\dot{f}_0$ [Hz s^{-1}]
GW250114	3.5	8.8	32.6	0.381	156.2	4.83×10^{-7}
GW250207	3.6	7.2	24.8	0.606	166.1	7.32×10^{-7}

long transients lasting hours to months, rather than persistent continuous-wave emission. Previous injection studies have shown that, for well-localized sources, using a single representative sky position is sufficient for this type of search because the targeted signals are relatively short and the sensitivity is only weakly affected by offsets within the localization region [67,79,80]. While the localization uncertainty differs between the two events, both are sufficiently well constrained to justify using a fixed sky position, without incurring the substantial computational cost of searching over a sky grid. Any residual sensitivity loss due to offsets from the true source position is consistently reflected in the sensitivity estimates of Sec. III E, where signal recovery is evaluated using the same fixed sky-position setup as in the search.

Following the guidelines in Ref. [79], we randomly draw 200 samples from the multidimensional posterior distribution of the remnant black hole. For each sample of black hole parameters and each boson mass considered in the search, we determine the optimal search configuration $(t_{\rm start}, T_{\rm coh}, T_{\rm obs})$, where $t_{\rm start}$ is the GPS start time of the search, corresponding to the time at which the cloud reaches saturation, and $T_{\rm obs}$ is the full search duration. We set $T_{\rm obs} = \tau^{\rm det}_{\rm GW}$, but typically cap it at 180 days to limit the computational cost of searching for suboptimally matched boson masses [67,119]. This cap, however, does not limit any of the search configurations used in this analysis, as detailed below. We then construct 11 representative search configurations by independently taking the 2nd, 10th, 20th, 30th, 40th, 50th, 60th, 70th, 80th, 90th, and 98th percentiles of the resulting marginal distributions of $t_{\rm start}$, $T_{\rm coh}$, and $T_{\rm obs}$. These configurations, summarized in Table IV for each event, are used in the HMM search, with the detector noise amplitude spectral densities estimated from the data over the corresponding coherent segments and searched frequency bands as part of the $\mathcal{F}$-statistic calculation [100]. No single configuration is optimal over the full parameter space because of the uncertainties in the remnant black-hole properties and the unknown boson mass, while using an individually optimized configuration for each parameter set would be computationally infeasible. We therefore use multiple configurations to balance broad coverage with search depth, improving sensitivity across the physically plausible signal parameter space while remaining computationally tractable. For most systems drawn from the remnant posterior distribution, the signal is expected to be recoverable by more than one configuration, making this percentile spacing a conservative choice.

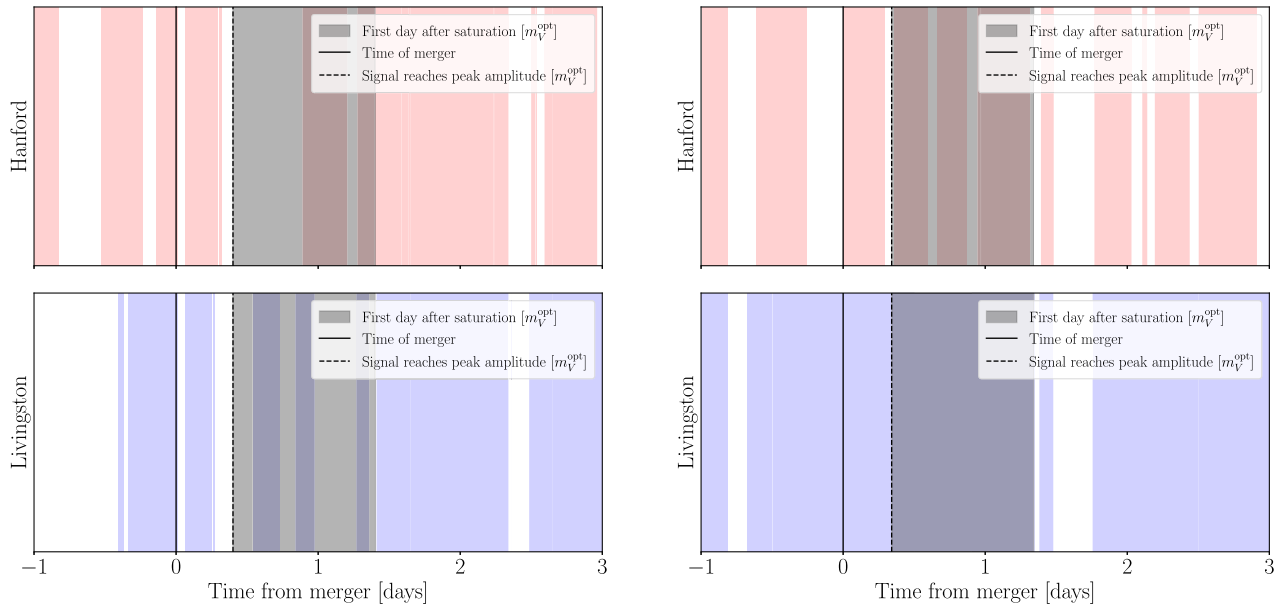
We exclude the configuration corresponding to the 98th percentile (configuration 11) from the analysis. This choice is motivated by the interplay between the expected signal persistence timescales and the O4c observing schedule. In particular, the longest-lived signals may extend to 13 May 2025 for GW250114 (GPS time 1431151905 s) and 11 May 2025 for GW250207 (GPS time 1431017883 s).

TABLE IV. Search configurations used in the HMM analysis of GW250114 (top) and GW250207 (bottom). For each configuration, we list the SFT duration $T_{\rm SFT}$, coherence time $T_{\rm coh}$, total observation time $T_{\rm obs}$, GPS start time, and the corresponding percentile.

%	$T_{\rm SFT}$ (min)	$T_{\rm coh}$ (min)	$T_{\rm obs}$ (min)	$t_{\rm start}$ (s)
2	3.45	13.8	1214.4	1420903701
10	3.90	15.6	1466.4	1420907361
20	4.30	17.2	1823.2	1420910601
30	4.90	19.6	2548.0	1420915521
40	6.15	24.6	3960.6	1420926381
50	8.25	33.0	6468.0	1420943481
60	11.55	46.2	11134.2	1420970601
70	16.85	67.4	20152.6	1421013921
80	25.75	103.0	38934.0	1421086281
90	27.80	166.8	80898.0	1421214441
2	2.85	11.4	946.2	1422985983
10	3.20	12.8	1126.4	1422988503
20	3.50	14.0	1428.0	1422990843
30	4.00	16.0	2000.0	1422995463
40	5.00	20.0	3060.0	1423004103
50	6.70	26.8	4931.2	1423017963
60	9.35	37.4	8452.4	1423040043
70	14.00	56.0	15792.0	1423078143
80	21.15	84.6	29948.4	1423136463
90	27.60	138.0	63756.0	1423246503

These intervals overlap with a scheduled commissioning break in O4c from 1 April 2025 to 11 June 2025 (GPS: 1427554818–1433689218), during which no observational data are available for coherent tracking over the full signal duration. We therefore omit this configuration to ensure consistency between the assumed signal evolution timescales and the data availability. The analysis is consequently performed over detector data spanning from 14 January 2025 to 15 March 2025 (GPS: 1420910601–1426068321) for GW250114 and from 7 February 2025 to 27 March 2025 (GPS: 1422988503–1427071863) for GW250207.

Over the full selected analysis intervals, the duty cycle for both events is ∼60%–70% in each detector. The HMM search itself naturally accommodates data gaps. During intervals with no available observational data, equal likelihoods are assigned to all frequency bins [79]. However, the temporal distribution of data availability differs between the two events, particularly in the early postmerger phase. In the first day after the expected superradiance saturation time, when the signal reaches its maximum amplitude for $m_V^{\rm opt}$, the duty cycle differs significantly between the events. For GW250114, the duty cycle is 44% in Hanford and 42% in Livingston, indicating intermittent coverage in either detector during the epoch of expected maximum signal strength and reducing the sensitivity of configurations targeting the shortest signals. In contrast, GW250207 has substantially higher coverage, with duty



(a) GW250114 (b) GW250207

FIG. 2. Data gaps in the LIGO Hanford and Livingston detectors relative to the merger times of GW250114 (a) and GW250207 (b). The red and blue shaded regions show the available data from Hanford and Livingston, respectively, while unshaded intervals indicate data gaps. The solid vertical line marks the merger time, while the dotted lines indicate the times at which the boson-cloud signal reaches peak amplitude for the optimal boson mass. The gray shaded region denotes the following one-day interval for the same optimal-boson-mass case. Time is shown in days relative to the merger.

cycles of 80.5% in Hanford and 99.7% in Livingston in the first day, corresponding to nearly continuous Livingston data and only limited gaps in Hanford, thereby reducing sensitivity loss during the same epoch. Data gaps around the merger time and over the subsequent three days, together with the peak signal times for $m_V^{\rm opt}$, are shown in Fig. 2.

D. Candidate follow-up

To distinguish potential signals from nonastrophysical artifacts, we implement a series of follow-up veto techniques following the framework described in Ref. [67]. A brief summary is provided here. All follow-up stages prior to manual inspection, including the initial candidate selection based on a detection-statistic threshold and the known-line and single-interferometer vetoes, are predefined and applied uniformly to all candidates.

In each 1 Hz band and for each search configuration, candidates are required to satisfy a threshold on the detection statistic, $\bar{\mathcal{L}} > \bar{\mathcal{L}}_{\rm th}$, where the threshold corresponds to a per-band, per-configuration false-alarm probability of 1%. The value of $\bar{\mathcal{L}}_{\rm th}$ is estimated empirically for each choice of $T_{\rm coh}$ using 300 realizations of Gaussian noise, taking the 99th percentile of the resulting distribution. Surviving candidates are then subjected to a known-line veto, in which the recovered Viterbi path is compared against the catalog of known instrumental lines in each detector and candidates with overlapping paths are rejected [67,120,121]. The remaining candidates are then subjected to a single-interferometer veto, followed by manual inspection.

For GW250114 and GW250207, the search spans 84 and 90 individual 1 Hz bands, respectively, and is carried out over 10 configurations, resulting in 840 and 900 optimal Viterbi paths, respectively. These paths correspond to the maximum-likelihood frequency-evolution tracks returned by the HMM tracking for each configuration in each 1 Hz subband [79,80]. After applying the initial threshold cut, the number of candidates is reduced to 52 for GW250114 and 64 for GW250207. The known-line veto [120,121] further reduces these to 3 and 12 candidates, respectively. We then apply a conservative single-interferometer veto by repeating the search using each detector individually. A candidate is vetoed if its detection statistic is below threshold in one detector but exceeds that of the multidetector search in the other detector, and the corresponding Viterbi paths overlap [67]. Such candidates are therefore consistent with detector-specific instrumental artifacts. This veto eliminates all remaining candidates for GW250114, while 10 candidates persist for GW250207. These remaining candidates are subsequently examined through manual inspection of the spectrograms from each detector in the relevant frequency band and time segments, to determine whether they overlap with any visible noise artifacts. All 10 candidates are found

TABLE V. Summary of candidate counts after each stage of the follow-up procedure for GW250114 and GW250207.

	Remaining candidates	
Stage	GW250114	GW250207
Initial candidates	52	64
Known-line veto	3	12
Single-IFO veto	0	10
Manual inspection	0	0

to coincide with detector-specific noise artifacts, predominantly in Hanford, and are therefore vetoed; see Appendix B for details of the manual inspection procedure and the spectrogram generation. A summary of the candidate counts at each stage of the follow-up procedure is provided in Table V, and a complete list of the vetoed candidates is provided in Ref. [122].

E. Disfavored parameter space

In the absence of detection, we derive the disfavored vector boson mass range using the method outlined in Ref. [67]. We estimate the search sensitivity via simulations. Synthetic signals are generated and injected into Gaussian noise realizations constructed to match real data, with amplitude spectral densities derived from detector data over the corresponding T_{obs} and 1 Hz subband (calculated from the harmonic mean over all the T_{SFT} segments), and with data gaps reproduced to reflect those present during the analysis period. Because these simulations use matched Gaussian noise realizations rather than injections into the exact measured detector noise, we refer to the resulting mass range as "disfavored" rather than strictly "excluded." We also avoid quoting conventional continuous-wave upper limits, since the search does not have a single, well-defined minimum detectable signal amplitude; the recovery probability depends on the remnant black-hole posteriors, the assumed boson mass, and the search configurations. For each assumed vector boson mass, we compute the detection probability by averaging the recovery efficiency over both noise realizations and posterior samples of the remnant black hole parameters, thereby accounting for their uncertainties. Specifically, following Ref. [67], we draw $N_{\mathrm{samp}} = 200$ samples from the posterior distribution of the remnant black hole parameters. For each posterior sample and assumed vector boson mass, a synthetic signal is generated and injected into $N_{\mathrm{noise}} = 10$ independent noise realizations. The recovery efficiency is then averaged over all posterior samples and noise realizations to obtain the detection probability [80],

$$P_{\mathrm{det}}(m_V) = \frac{1}{N_{\mathrm{samp}} N_{\mathrm{noise}}} \sum_{i=1}^{N_{\mathrm{samp}}} N_{\mathrm{det}}(\theta_i; m_V), \qquad (2)$$

where θ_i denotes a sampled set of black hole parameters and $N_{\mathrm{det}}(\theta_i; m_V)$ is the number of recovered signals out of the N_{noise} noise realizations for that sample. Simulations are performed for all search configurations used in the analysis, and a signal is considered recovered if at least one configuration yields a detection statistic above the chosen threshold. Only this threshold-based candidate selection is applied to the simulations; the subsequent follow-up vetoes used in the search are not included. Some persistent narrow-band instrumental lines fall within the frequency ranges of both searches and appear as localized non-Gaussian features, although they correspond to slightly different boson masses because of the different source redshifts. The resulting detection probabilities may therefore be somewhat optimistic in frequency bands affected by known lines and non-Gaussian noise artifacts, and the quoted disfavored mass ranges should be interpreted as most robust where the detector noise is well approximated by Gaussian noise.

The resulting detection probability $P_{\mathrm{det}}(m_V)$ quantifies the likelihood that a signal would have been detected by our pipeline if present. In the absence of detection, this quantity can be interpreted as the confidence level at which a given boson mass is disfavored. Although the two events probe similar vector-boson mass ranges, GW250207 yields strong confidence near m_V^{opt}, where the expected signals are the shortest, whereas GW250114 lacks sensitivity to these shortest-duration signals due to data gaps during the corresponding early-time interval. For a false alarm probability of $P_{\mathrm{fa}} = 1\%$, we disfavor vector boson mass ranges of $[2.80, 3.26] \times 10^{-13}$ eV for GW250114 and $[2.83, 3.95] \times 10^{-13}$ eV for GW250207 at 90% confidence, as shown in Fig. 3. We quote a combined interval of $[2.80, 3.95] \times 10^{-13}$ eV, defined as the union of these independently disfavored mass ranges rather than as the result of a joint statistical combination of the two searches. We also include one simulation-only point above the upper boundary of the searched mass range for GW250207 (connected by the dashed line) to verify the expected decrease in P_{det} at higher vector-boson masses. This point is not part of the search and is not used to define the disfavored mass range.

These results can be compared with those obtained in the O4a analysis of Ref. [67] (see Fig. 3 therein), where the disfavored mass ranges for GW230814 and GW231123 were reported at a lower confidence level of ∼30% for $P_{\mathrm{fa}} = 1\%$. The higher confidence achieved with GW250114 and GW250207 here is primarily driven by their closer distance, higher signal-to-noise ratios, and tighter constraints on source parameters. Improved sky localization reduces the parameter space explored by the search, while smaller luminosity distances increase the expected signal amplitude. In particular, GW250207 is located at a distance of ∼187 Mpc, significantly closer than typical O4a events [97], leading to a higher recovery

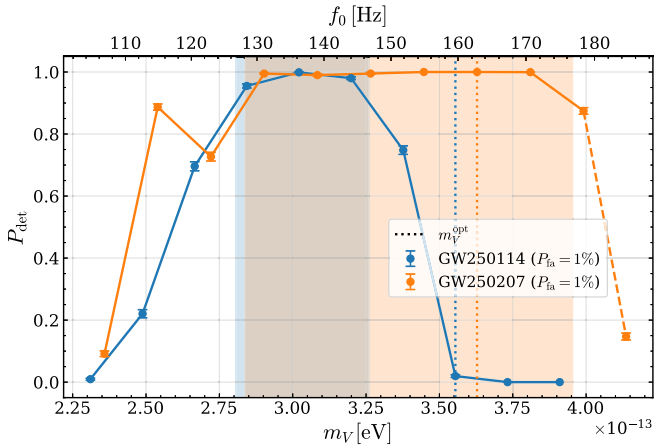


FIG. 3. Detection probability $P_{\rm det}$ as a function of vector boson mass m_V (bottom axis) and the corresponding gravitational wave frequency in the detector frame (top axis), with a 1% false alarm probability ($P_{\rm fa}$), for the remnant black holes formed in GW250114 (blue) and GW250207 (orange). The vertical dotted lines mark the optimal boson masses $m_V^{\rm opt}$ for the remnants with median parameters listed in Table I. The shaded region corresponds to the disfavored boson mass range with greater than 90% confidence. The dashed segment indicates a simulation-only extension beyond the searched mass range for GW250207, included to verify that $P_{\rm det}$ decreases at higher boson masses. The error bars represent the 1σ beta-binomial uncertainty in $P_{\rm det}$ [123]; some are smaller than the marker size and are therefore not visible. (The top-axis frequencies are obtained by averaging f_0 over search configurations for each boson mass, using the median black-hole parameters in Table I; the two events give nearly identical frequency mappings.)

efficiency and consequently stronger constraints on the vector boson mass.

IV. CONSTRAINTS FROM PREMERGER BLACK HOLES

A. Method

In addition to the directed HMM searches, we implement a complementary method to constrain ultralight bosons (scalar and vector) using spin measurements of binary black hole merger events, following Ref. [48]. This method exploits the fact that superradiant instabilities impose an upper bound on black hole spin for a given boson mass. If ultralight bosons of mass m_b exist, black holes can undergo superradiant spin-down over a characteristic timescale $\tau_{\rm growth}(M,\chi,m_b)$. For systems with age $T_{\rm age} \gtrsim \tau_{\rm growth}$, this leads to a maximum allowed spin $\chi_{\rm max}(M,m_b,T_{\rm age})$, defining an excluded region in the mass-spin plane.

We compute $\chi_{\rm max}$ using the SuperRad package [40,102], assuming conservatively that the cloud grows from vacuum fluctuations to the saturation mass at which the instability shuts off. We include fully relativistic superradiant frequencies and instability rates for dominant modes with $m \leq 2$ and adopt nonrelativistic approximations for higher modes as described in Ref. [48].

The efficiency of superradiant spin-down depends on the elapsed time between black-hole formation and merger. Following Refs. [48,50], we consider $T_{\rm age} \in [10^5, 10^7]$ yr, where the lower bound is motivated by merger timescales for dynamically formed binaries in a dense environment, and the upper bound is adopted as a representative inspiral timescale for isolated binary evolution [124–126]. The exclusion region expands with $T_{\rm age}$, since older black holes would have undergone superradiant spin-down for a longer time, thereby strengthening the constraints on the boson mass, although the dependence is not strong over this range. We neglect possible perturbative effects of the binary companion on cloud growth, so $T_{\rm age}$ should be interpreted as a lower bound on the time available for superradiance prior to binary interaction suppressing the instability.

For each merger event, we use posterior samples from the event parameter estimation. Denoting the primary black-hole mass and dimensionless spin by $m_1^{(i)}$ and $\chi_1^{(i)}$ we compute the posterior-driven nonexclusion probability

$$P(m_b, T_{\rm age}) = \frac{1}{N_{\rm samp}} \sum_{i=1}^{N_{\rm samp}} I\{\chi_1^{(i)} < \chi_{\rm max}(m_1^{(i)}, m_b, T_{\rm age})\}, \tag{3}$$

where $I\{\cdot\}$ is an indicator function that returns unity if the primary BH spin lies below its respective superradiance-imposed upper bound $\chi_{\rm max}$, and zero otherwise, and $N_{\rm samp} \sim \mathcal{O}(10^4)$ is the number of posterior samples. We restrict the reported constraints to the primary components, though in principle, information about the secondary spin could extend the constraints. For the systems considered here, the secondary spin posteriors remain close to their priors and are largely uninformative. Applying the exclusion criterion defined below to the secondary components individually yields no excluded boson-mass intervals for the black-hole ages considered here. Jointly using both component spins while taking into account their correlations could still strengthen the constraints, though we conservatively do not consider that here.

We also account for the possibility that the exclusion could be influenced by the spin prior rather than by the data. In some regions of parameter space, the maximum allowed spin after superradiant spin-down, $\chi_{\rm max}$, can be sufficiently small that it removes a non-negligible fraction of the prior support. To quantify this effect, we compute a prior-driven non-exclusion probability, $P'(m_b, T_{\rm age})$, using the same procedure as for $P(m_b, T_{\rm age})$, but drawing χ_1 directly from the uniform spin prior (consistent with the spin priors adopted in GWTC-5 [85]). We then regard a boson mass m_b as excluded at least at 90% confidence for a given spin-down timescale $T_{\rm age}$ only if

$$P(m_b, T_{\rm age}) < 0.1P'(m_b, T_{\rm age}). \quad (4)$$

This requirement is more conservative than the nominal criterion $P(m_b, T_{\rm age}) < 0.1$, because it demands that the posterior-based nonexclusion probability be reduced by more than a factor of 10 relative to the prior-only expectation. In this way, the inferred constraint is required to be driven by the measured spin information rather than by the assumed uniform spin prior. More details are provided in Ref. [48].

B. Results

We apply the spin-based superradiance framework described in Sec. IV to three O4b events: GW240515, GW241113, and GW241225_08. The resulting exclusion regions in boson mass are shown in Fig. 4, where shaded areas correspond to parameters excluded at 90% confidence. Separate analyses are performed for scalar and vector bosons. Assuming a black-hole age of $T_{\rm age} = 10^5$ yr, we exclude scalar bosons in the mass range $[1.39, 6.94] \times 10^{-13}$ eV and vector bosons in the mass range $[0.32, 14.4] \times 10^{-13}$ eV at 90% confidence. These quoted intervals are constructed as the union of the event-by-event excluded mass ranges from the three O4b events shown in Fig. 4. The excluded region broadens with increasing assumed black-hole age.

The excluded mass ranges obtained here are broadly consistent with those previously reported for individual high-spin events in earlier studies [48,50] (marked by red lines in Fig. 4, assuming a black-hole age of $T_{\rm age} = 10^5$ yr). The stronger constraints from previous events arise from a combination of better-constrained spins for lower-mass black holes and the inclusion of higher-mass black holes, which extend the range of boson masses that can be excluded. This is expected because these constraints are driven primarily by the constituent black-hole masses and spins, rather than by detector sensitivity alone. The events with well-constrained high spins considered so far have mostly fallen within a similar black-hole mass range and therefore probe a similar boson mass range where the detectors are most sensitive. As additional high-spin mergers are observed with a wider spread in black hole masses, the excluded region in boson parameter space will continue to expand. The vector-boson exclusions obtained from these three events span a broader boson mass range than the disfavored region from the directed searches presented in Sec. III, including that region while extending to lower and higher boson masses. Both approaches strongly disfavor vector bosons with masses $\sim 10^{-13}$ eV.

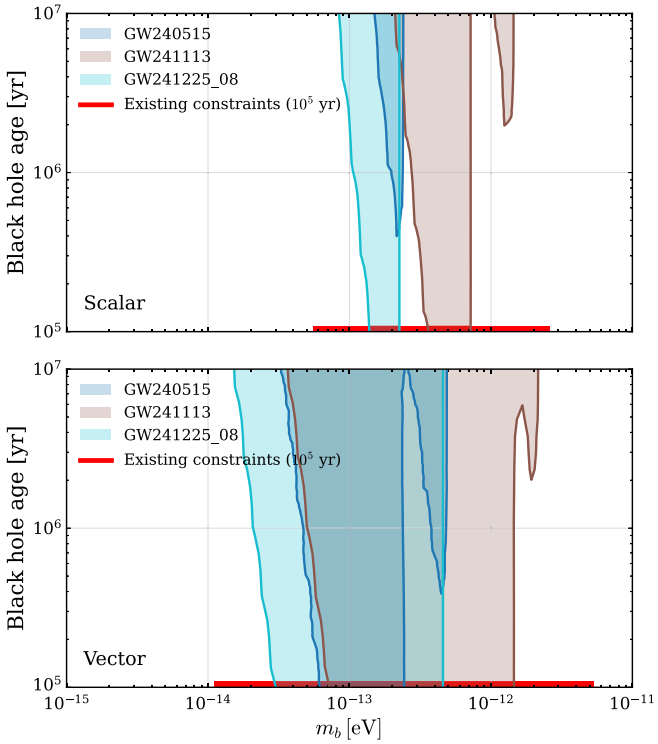


FIG. 4. Exclusion regions for scalar and vector boson masses as a function of the black hole age, inferred from the primary black hole spin measurements in the three binaries. The shaded regions are excluded by each event at confidence levels above 90% (i.e., $P < 0.1P'$) [48]. The red line indicates the conservative boson mass range previously excluded using the same technique [48,50], assuming a black hole lifetime of $T_{\rm age} = 10^5$ yr.

V. CONCLUSIONS

In this study, we present two complementary approaches to probe ultralight bosons using gravitational-wave observations: directed searches for vector boson cloud emission from merger remnants and constraints derived from high-spin measurements of pre-merger constituent black holes (for scalar and vector bosons). These methods yield consistent and complementary constraints on the boson parameter space.

The directed HMM searches target newly formed merger remnants, where boson clouds may form and emit gravitational waves on timescales of hours to months. No evidence of the signal is found in searches targeting the remnants of two loud merger events, GW250114 and GW250207. The disfavored vector boson mass ranges are derived with high confidence around 3×10^{-13} eV. These results demonstrate the increasing sensitivity of directed searches as detector performance improves and louder events become available.

The spin-based analysis provides an independent constraint by leveraging the absence of superradiant spin-down in highly spinning pre-merger black holes. By analyzing three O4b events, we obtain exclusion regions for both scalar and vector bosons that are consistent with previous constraints from high-spin constituent black holes. The vector-boson exclusions are also broadly consistent with

the disfavored range from the directed searches in this study, while extending to higher vector-boson masses.

The two approaches are complementary in both methodology and astrophysical interpretation. The directed search probes the presence of boson clouds around recently formed black holes, with minimal dependence on assumptions about binary evolution, whereas the spin-based constraints rely on the long-term evolution of black holes and are subject to astrophysical uncertainties. Therefore, the two methods, while covering overlapping regions of parameter space, provide complementary observational probes of vector bosons based on distinct assumptions.

Continued improvements in detector sensitivity, together with the accumulation of high signal-to-noise ratio events, will enhance the reach of both approaches. In particular, the identification of additional nearby merger remnants and highly spinning black holes will further expand the excluded regions in boson parameter space. Combined analyses that integrate multiple events and jointly model boson cloud dynamics and spin evolution may offer a powerful avenue for future studies.

ACKNOWLEDGMENTS

This material is based upon work supported by NSF's LIGO Laboratory, which is a major facility fully funded by the National Science Foundation. The authors also gratefully acknowledge the support of the Science and Technology Facilities Council (STFC) of the United Kingdom, the Max-Planck-Society (MPS), and the State of Niedersachsen/Germany for support of the construction of Advanced LIGO and construction and operation of the GEO 600 detector. Additional support for Advanced LIGO was provided by the Australian Research Council. The authors gratefully acknowledge the Italian Istituto Nazionale di Fisica Nucleare (INFN), the French Centre National de la Recherche Scientifique (CNRS) and the Netherlands Organization for Scientific Research (NWO) for the construction and operation of the Virgo detector and the creation and support of the EGO consortium. The authors also gratefully acknowledge research support from these agencies as well as by the Council of Scientific and Industrial Research of India, the Department of Science and Technology, India, the Science & Engineering Research Board (SERB), India, the Ministry of Human Resource Development, India, the Spanish Agencia Estatal de Investigación (AEI), the Spanish Ministerio de Ciencia, Innovación y Universidades, the European Union NextGenerationEU/PRTR (PRTR-C17.I1), the ICSC–Centro Nazionale di Ricerca in High Performance Computing, Big Data and Quantum Computing, funded by the European Union NextGenerationEU, the Comunitat Autonòma de les Illes Balears through the Conselleria d'Educació i Universitats, the Conselleria d'Innovació, Universitats, Ciència i Societat Digital de la Generalitat Valenciana and the CERCA Programme Generalitat de Catalunya, Spain, the Polish National Agency for Academic Exchange, the National Science Centre of Poland and the European Union—European Regional Development Fund; the Foundation for Polish Science (FNP), the Polish Ministry of Science and Higher Education, the Swiss National Science Foundation (SNSF), the Russian Science Foundation, the European Commission, the European Social Funds (ESF), the European Regional Development Funds (ERDF), the Royal Society, the Scottish Funding Council, the Scottish Universities Physics Alliance, the Hungarian Scientific Research Fund (OTKA), the French Lyon Institute of Origins (LIO), the Belgian Fonds de la Recherche Scientifique (FRS-FNRS), Actions de Recherche Concertées (ARC) and Fonds Wetenschappelijk Onderzoek—Vlaanderen (FWO), Belgium, the Paris Île-de-France Region, the National Research, Development and Innovation Office of Hungary (NKFIH), the National Research Foundation of Korea, the Natural Sciences and Engineering Research Council of Canada (NSERC), the Canadian Foundation for Innovation (CFI), the Brazilian Ministry of Science, Technology, and Innovations, the International Center for Theoretical Physics South American Institute for Fundamental Research (ICTP-SAIFR), the Research Grants Council of Hong Kong, the National Natural Science Foundation of China (NSFC), the Israel Science Foundation (ISF), the U.S.-Israel Binational Science Fund (BSF), the Leverhulme Trust, the Research Corporation, the National Science and Technology Council (NSTC), Taiwan, the United States Department of Energy, and the Kavli Foundation. The authors gratefully acknowledge the support of the NSF, STFC, INFN and CNRS for provision of computational resources. This work was supported by MEXT, the JSPS Leading-edge Research Infrastructure Program, JSPS Grant-in-Aid for Specially Promoted Research 26000005, JSPS Grant-in-Aid for Scientific Research on Innovative Areas 2402: No. 24103006, No. 24103005, and 2905: No. JP17H06358, No. JP17H06361, and No. JP17H06364, JSPS Core-to-Core Program A. Advanced Research Networks, JSPS Grants-in-Aid for Scientific Research (S) No. 17H06133, 20H05639, and No. 26K21721, JSPS Grant-in-Aid for Transformative Research Areas (A) 26A204: No. JP26H00407, the joint research program of the Institute for Cosmic Ray Research, University of Tokyo, the National Research Foundation (NRF), the Computing Infrastructure Project of the Global Science experimental Data hub Center (GSDC) at KISTI, the Korea Astronomy and Space Science Institute (KASI), the Ministry of Science and ICT (MSIT) in Korea, Academia Sinica (AS), the AS Grid Center (ASGC) and the National Science and Technology Council (NSTC) in Taiwan under grants including the Science Vanguard Research Program, the Advanced Technology Center (ATC) of NAOJ, the

Mechanical Engineering Center of KEK and Vietnam National Foundation for Science and Technology Development (NAFOSTED) No. 103.01-2025.147. Additional acknowledgments for support of individual authors may be found in the following document: [127].

DATA AVAILABILITY

The data that support the findings of this article are openly available [122].

APPENDIX A: VECTOR BOSON SIGNAL MODEL FOR REMNANT BLACK HOLES

Using the SuperRad waveform model [40,102] and the median remnant masses and spins listed in Table I, we determine, for each system, the vector boson mass that maximizes the superradiant instability. This optimal mass, m_V^{opt}, yields the largest gravitational-wave strain amplitude attainable by a given black hole-boson system at a reference time t_{ref}, defined as the time at which the boson cloud reaches its full growth and the instability saturates.

For each remnant, SuperRad is used to compute the corresponding gravitational-wave signal parameters, including the cloud growth timescale τ_{growth}, the emission (depletion) timescale τ_{GW}, the strain amplitude h_0, the time-dependent emission frequency f_{GW} and the frequency derivative $\dot{f}_{\mathrm{GW}}$.

The initial gravitational-wave frequency in the source frame is set by the angular frequency of the saturated cloud, $f = \omega/\pi$, while its subsequent evolution can be approximated as,

$$f_{\mathrm{GW}}(t) = f_\infty - \frac{|f_{\mathrm{shift}}|}{1 + (t - t_{\mathrm{sat}})/\tau_{\mathrm{GW}}}, \tag{A1}$$

where f_∞ is the asymptotic frequency at late times and f_{shift} accounts for the initial self-gravity of the cloud. In practice, SuperRad incorporates higher-order relativistic corrections to compute f_{GW} and $\dot{f}_{\mathrm{GW}}$ with high accuracy.

As both search targets are merger remnants at cosmological distances, we account for redshift effects when mapping to the detector frame. The observed gravitational-wave frequency and its derivative scale as

$$f_{\mathrm{det}} = \frac{f_{\mathrm{src}}}{1+z}, \qquad \dot{f}_{\mathrm{det}} = \frac{\dot{f}_{\mathrm{src}}}{(1+z)^2}, \tag{A2}$$

while the emission timescale is correspondingly dilated,

$$\tau_{\mathrm{GW}}^{\mathrm{det}} = (1+z)\tau_{\mathrm{GW}}^{\mathrm{src}}, \tag{A3}$$

where the superscripts "src" and "det" denote the source and detector frames, respectively.

TABLE VI. Start frequencies, search configurations, and detection statistics of the 10 candidates subjected to manual inspection for GW250207.

f_0 (Hz)	t_{start} (s)	T_{coh} (min)	T_{obs} (min)	$\bar{\mathcal{L}}$
176.81	1422985983	11.4	946.2	7.48
178.97	1422985983	11.4	946.2	7.54
145.04	1422988503	12.8	1126.4	8.48
176.82	1422988503	12.8	1126.4	7.51
178.97	1422988503	12.8	1126.4	7.47
145.04	1422990843	14.0	1428.0	8.08
176.79	1422990843	14.0	1428.0	7.42
178.63	1422990843	14.0	1428.0	7.23
176.79	1423004103	20.0	3060.0	7.24
144.97	1423136463	84.6	29948.4	6.71

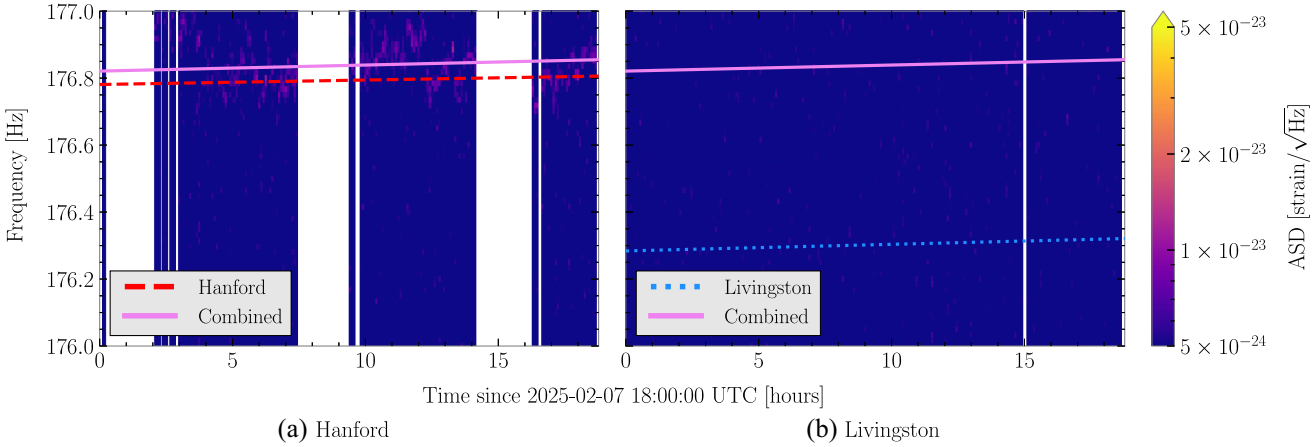
APPENDIX B: MANUAL INSPECTION OF FINAL CANDIDATES

The manual inspection is performed using spectrograms generated from calibrated strain data. The spectrograms are constructed using the Welch method by averaging 60-s Fourier transforms over the inspected duration, corresponding to a frequency resolution of approximately 0.017 Hz. To ensure consistency with the HMM search, only analysis-ready data segments included in the search are used to construct the spectrograms.

All 10 remaining candidates for GW250207 overlap with noise artifacts visible in the spectrograms, predominantly in the Hanford detector. The surviving candidates' starting frequencies, search configurations, and detection statistics are listed in Table VI. In this section, we present representative examples illustrating the basis for their veto.

For each candidate, spectrograms from the Hanford and Livingston detectors are examined in the relevant frequency sub-band and time segment. A common pattern is observed across all surviving candidates: the candidate tracks coincide with visible wandering noise features in the Hanford data, while the corresponding Livingston spectrograms remain comparatively free of similar features. Furthermore, the optimal paths recovered from the combined Hanford-Livingston data generally lie close to those from the Hanford data alone, indicating that the candidate significance is dominated by detector-specific artifacts rather than coherent excess power present in both detectors.

Figure 5 shows a representative example corresponding to a candidate with $f_0 = 176.82$ Hz, $t_{\mathrm{start}} = 1422988503$ s, $T_{\mathrm{coh}} = 12.8$ min, and $T_{\mathrm{obs}} \approx 19$ h. A weak noise track can be seen near the recovered track, whereas no comparable structure is present in the Livingston data. The optimal path obtained by combining data from both detectors closely follows the Hanford-only path, consistent with a detector-specific noise artifact. Similar behavior is observed for the remaining candidates. The gaps visible in the spectrograms



(a) Hanford (b) Livingston

FIG. 5. Representative example of a candidate vetoed during manual inspection. The (a) and (b) panels show the Hanford and Livingston spectrograms, respectively. The red dashed, blue dotted, and magenta solid tracks denote the optimal paths obtained from Hanford-only, Livingston-only, and combined Hanford-Livingston data, respectively. Gaps in the spectrograms correspond to intervals that were not analysis ready and were therefore excluded from the search.

correspond to intervals that were not analysis-ready and were therefore excluded from both the HMM search and the spectrogram.

[1] G. Bertone and T. M. P. Tait, Nature (London) **562**, 51 (2018).
[2] G. Bertone and D. Hooper, Rev. Mod. Phys. **90**, 045002 (2018).
[3] E. Oks, New Astron. Rev. **93**, 101632 (2021).
[4] M. Baryakhtar, L. Rosenberg, and G. Rybka, Rep. Prog. Phys. **88**, 106901 (2025).
[5] A. Arvanitaki, S. Dimopoulos, S. Dubovsky, N. Kaloper, and J. March-Russell, Phys. Rev. D **81**, 123530 (2010).
[6] F. F. Freitas, C. A. Herdeiro, A. P. Morais, A. Onofre, R. Pasechnik, E. Radu, N. Sanchis-Gual, and R. Santos, J. Cosmol. Astropart. Phys. 12 (2021) 047.
[7] B. Holdom, Phys. Lett. **166B**, 196 (1986).
[8] M. Goodsell, J. Jaeckel, J. Redondo, and A. Ringwald, J. High Energy Phys. 11 (2009) 027.
[9] J. Jaeckel and A. Ringwald, Annu. Rev. Nucl. Part. Sci. **60**, 405 (2010).
[10] R. Essig *et al.*, in Snowmass 2013: Snowmass on the Mississippi (2013) arXiv:1311.0029.
[11] P. Agrawal, N. Kitajima, M. Reece, T. Sekiguchi, and F. Takahashi, Phys. Lett. B **801**, 135136 (2020).
[12] M. Fabbrichesi, E. Gabrielli, and G. Lanfranchi, *The Physics of the Dark Photon* (Springer International Publishing, Cham, 2021).
[13] A. Arvanitaki and S. Dubovsky, Phys. Rev. D **83**, 044026 (2011).
[14] H. Yoshino and H. Kodama, Prog. Theor. Exp. Phys. **2014**, 043E02 (2014).
[15] H. Yoshino and H. Kodama, Prog. Theor. Exp. Phys. **2015**, 061E01 (2015).
[16] A. Arvanitaki, M. Baryakhtar, and X. Huang, Phys. Rev. D **91**, 084011 (2015).
[17] A. Arvanitaki, M. Baryakhtar, S. Dimopoulos, S. Dubovsky, and R. Lasenby, Phys. Rev. D **95**, 043001 (2017).
[18] R. Brito, S. Ghosh, E. Barausse, E. Berti, V. Cardoso, I. Dvorkin, A. Klein, and P. Pani, Phys. Rev. Lett. **119**, 131101 (2017).
[19] R. Brito, S. Ghosh, E. Barausse, E. Berti, V. Cardoso, I. Dvorkin, A. Klein, and P. Pani, Phys. Rev. D **96**, 064050 (2017).
[20] M. Baryakhtar, R. Lasenby, and M. Teo, Phys. Rev. D **96**, 035019 (2017).
[21] K. H. M. Chan and O. A. Hannuksela, Phys. Rev. D **109**, 023009 (2024).
[22] V. Cardoso, Óscar J. C. Dias, G. S. Hartnett, M. Middleton, P. Pani, and J. E. Santos, J. Cosmol. Astropart. Phys. 03 (2018) 043.
[23] D. Baumann, H. S. Chia, and R. A. Porto, Phys. Rev. D **99**, 044001 (2019).
[24] O. A. Hannuksela, K. W. K. Wong, R. Brito, E. Berti, and T. G. F. Li, Nat. Astron. **3**, 447 (2019).
[25] J. Zhang and H. Yang, Phys. Rev. D **99**, 064018 (2019).
[26] W. E. East, Phys. Rev. D **96**, 024004 (2017).
[27] W. E. East and F. Pretorius, Phys. Rev. Lett. **119**, 041101 (2017).
[28] W. E. East, Phys. Rev. Lett. **121**, 131104 (2018).
[29] N. Siemonsen and W. E. East, Phys. Rev. D **101**, 024019 (2020).
[30] R. Brito, V. Cardoso, and P. Pani, Lect. Notes Phys. **971**, 1 (2020).

[31] Ya. B. Zel'dovich, JETP Lett. **14**, 180 (1971).
[32] A. A. Starobinsky, Sov. Phys. JETP **37**, 28 (1973).
[33] S. Detweiler, Phys. Rev. D **22**, 2323 (1980).
[34] J. D. Bekenstein, Phys. Rev. D **7**, 949 (1973).
[35] S. R. Dolan, Phys. Rev. D **76**, 084001 (2007).
[36] C. A. Herdeiro, E. Radu, and N. M. Santos, Phys. Lett. B **824**, 136835 (2022).
[37] M. Isi, L. Sun, R. Brito, and A. Melatos, Phys. Rev. D **99**, 084042 (2019).
[38] M. Baryakhtar, M. Galanis, R. Lasenby, and O. Simon, Phys. Rev. D **103**, 095019 (2021).
[39] N. Siemonsen, C. Mondino, D. Egaña Ugrinovic, J. Huang, M. Baryakhtar, and W. E. East, Phys. Rev. D **107**, 075025 (2023).
[40] T. May, W. E. East, and N. Siemonsen, Phys. Rev. D **111**, 044062 (2025).
[41] J. Aasi *et al.* (LIGO Scientific Collaboration), Classical Quantum Gravity **32**, 074001 (2015).
[42] F. Acernese *et al.* (Virgo Collaboration), Classical Quantum Gravity **32**, 024001 (2014).
[43] T. Akutsu *et al.* (KAGRA Collaboration), Prog. Theor. Exp. Phys. **2021**, 05A101 (2020).
[44] B. P. Abbott *et al.* (LIGO Scientific, Virgo, and KAGRA Collaborations), Living Rev. Relativity **23**, 3 (2020).
[45] A. Abac *et al.* (ET Collaboration), J. Cosmol. Astropart. Phys. 03 (2026) 081.
[46] M. Evans *et al.*, arXiv:2109.09882.
[47] K. K. Y. Ng, S. Vitale, O. A. Hannuksela, and T. G. F. Li, Phys. Rev. Lett. **126**, 151102 (2021).
[48] P. S. Aswathi, W. E. East, N. Siemonsen, L. Sun, and D. Jones, Phys. Rev. D **112**, 123048 (2025).
[49] A. Caputo, G. Franciolini, and S. J. Witte, Phys. Rev. D **113**, 083031 (2026).
[50] A. G. Abac *et al.* (LIGO Scientific, Virgo, and KAGRA Collaborations), Astrophys. J. Lett. **993**, L21 (2025).
[51] O. Ning, B. R. Safdi, and C. Welch, arXiv:2607.01317.
[52] S. J. Witte and A. Mummery, Phys. Rev. D **111**, 083044 (2025).
[53] A. Mummery, J. Jiang, A. Ingram, A. Fabian, and J. Rule, Mon. Not. R. Astron. Soc. **544**, 2880 (2025).
[54] C. S. Reynolds, Nat. Astron. **3**, 41 (2019).
[55] J. E. McClintock, R. Narayan, and J. F. Steiner, Space Sci. Rev. **183**, 295 (2014).
[56] R. Abbott *et al.* (LIGO Scientific, Virgo, and KAGRA Collaborations), Phys. Rev. D **105**, 102001 (2022).
[57] C. Palomba *et al.*, Phys. Rev. Lett. **123**, 171101 (2019).
[58] V. Dergachev and M. A. Papa, Phys. Rev. Lett. **123**, 101101 (2019).
[59] R. Abbott *et al.* (LIGO Scientific, Virgo, and KAGRA Collaborations), Phys. Rev. D **106**, 042003 (2022).
[60] S. J. Zhu, M. Baryakhtar, M. A. Papa, D. Tsuna, N. Kawanaka, and H.-B. Eggenstein, Phys. Rev. D **102**, 063020 (2020).
[61] S. A. R. Ellis, O. Ning, N. L. Rodd, and J. Schütte-Engel, arXiv:2603.15734.
[62] L. Tsukada, T. Callister, A. Matas, and P. Meyers, Phys. Rev. D **99**, 103015 (2019).
[63] C. Yuan, Y. Jiang, and Q.-G. Huang, Phys. Rev. D **106**, 023020 (2022).
[64] L. Tsukada, R. Brito, W. E. East, and N. Siemonsen, Phys. Rev. D **103**, 083005 (2021).
[65] L. Sun, R. Brito, and M. Isi, Phys. Rev. D **101**, 063020 (2020).
[66] S. Collaviti, L. Sun, M. Galanis, and M. Baryakhtar, Classical Quantum Gravity **42**, 025006 (2024).
[67] A. G. Abac *et al.* (The LIGO Scientific, the Virgo, and the KAGRA Collaborations), Phys. Rev. D **114**, 022006 (2026).
[68] L. Mirasola, C. Mondino, F. Amicucci, N. Siemonsen, C. Palomba, S. D'Antonio, P. Leaci, L. D'Onofrio, P. Astone, D. Egaña-Ugrinovic, J. Huang, M. Baryakhtar, and W. E. East, Phys. Rev. D **111**, 084032 (2025).
[69] S. M. Vermeulen *et al.*, Nature (London) **600**, 424 (2021).
[70] A. S. Göttel, A. Ejlli, K. Karan, S. M. Vermeulen, L. Aiello, V. Raymond, and H. Grote, Phys. Rev. Lett. **133**, 101001 (2024).
[71] L. Aiello, J. W. Richardson, S. M. Vermeulen, H. Grote, C. Hogan, O. Kwon, and C. Stoughton, Phys. Rev. Lett. **128**, 121101 (2022).
[72] A. G. Abac *et al.* (LIGO Scientific, Virgo, and KAGRA Collaborations), Phys. Rev. Lett. **137**, 131001 (2026).
[73] R. Abbott *et al.* (LIGO Scientific, Virgo, and KAGRA Collaborations), Phys. Rev. D **105**, 063030 (2022).
[74] A. G. Abac *et al.* (LIGO Scientific, Virgo, and KAGRA Collaborations), Phys. Rev. D **110**, 042001 (2024).
[75] Q. Yang, L.-W. Ji, B. Hu, Z.-J. Cao, and R.-G. Cai, Res. Astron. Astrophys. **18**, 065 (2018).
[76] S. Choudhary, N. Sanchis-Gual, A. Gupta, J. C. Degollado, S. Bose, and J. A. Font, Phys. Rev. D **103**, 044032 (2021).
[77] S. Roy, R. Vicente, J. C. Aurrekoetxea, K. Clough, and P. G. Ferreira, Phys. Rev. Lett. **136**, 191402 (2026).
[78] G. M. Tomaselli, T. F. M. Spieksma, and G. Bertone, Phys. Rev. Lett. **133**, 121402 (2024).
[79] D. Jones, L. Sun, N. Siemonsen, W. E. East, S. M. Scott, and K. Wette, Phys. Rev. D **108**, 064001 (2023).
[80] D. Jones, N. Siemonsen, L. Sun, W. E. East, A. L. Miller, K. Wette, and O. J. Piccinni, Phys. Rev. D **111**, 063028 (2025).
[81] S. Ghosh, E. Berti, R. Brito, and M. Richartz, Phys. Rev. D **99**, 104030 (2019).
[82] A. G. Abac *et al.* (LIGO Scientific, Virgo, and KAGRA Collaborations), arXiv:2605.27225.
[83] A. G. Abac *et al.* (LIGO Scientific, Virgo, and KAGRA Collaborations), Phys. Rev. Lett. **137**, 071401 (2026).
[84] A. G. Abac *et al.* (LIGO Scientific, Virgo, and KAGRA Collaborations), arXiv:2605.27223.
[85] A. G. Abac *et al.* (LIGO Scientific, Virgo, and KAGRA Collaborations), arXiv:2605.27224.
[86] B. Moe, P. Brady, B. Stephens, E. Katsavounidis, R. Williams, and F. Zhang, GraceDB: A gravitational wave candidate event database, (2014) https://dcc.ligo.org/LIGO-T1400365/public.
[87] LIGO Scientific, Virgo, and KAGRA Collaborations, Zenodo (2026), 10.5281/zenodo.20348005.
[88] LIGO Scientific, Virgo, and KAGRA Collaborations, Zenodo (2026), 10.5281/zenodo.20348006.
[89] A. G. Abac, I. Abouelfettouh, F. Acernese *et al.* (LIGO Scientific, Virgo, and KAGRA Collaborations), Phys. Rev. Lett. **135**, 111403 (2025).

[90] A. G. Abac *et al.* (LIGO Scientific, Virgo, and KAGRA Collaborations), Phys. Rev. Lett. **136**, 041403 (2026).
[91] V. Varma, S. E. Field, M. A. Scheel, J. Blackman, D. Gerosa, L. C. Stein, L. E. Kidder, and H. P. Pfeiffer, Phys. Rev. Res. **1**, 033015 (2019).
[92] G. Ashton *et al.*, Astrophys. J. Suppl. Ser. **241**, 27 (2019).
[93] I. M. Romero-Shaw *et al.*, Mon. Not. R. Astron. Soc. **499**, 3295 (2020).
[94] J. S. Speagle, Mon. Not. R. Astron. Soc. **493**, 3132 (2020).
[95] M. Colleoni, F. A. Ramis Vidal, C. García-Quirós, S. Akçay, and S. Bera, Phys. Rev. D **111**, 104019 (2025).
[96] G. Pratten *et al.*, Phys. Rev. D **103**, 104056 (2021).
[97] LIGO Scientific, Virgo, and KAGRA Collaborations, Astrophys. J. Lett. **1004**, L22 (2026).
[98] P. Jaranowski, A. Królak, and B. F. Schutz, Phys. Rev. D **58**, 063001 (1998).
[99] C. Cutler and B. F. Schutz, Phys. Rev. D **72**, 063006 (2005).
[100] R. Prix, The F-statistic and its implementation in ComputeFStatistic v2, Technical Report, LIGO-T0900149-v3 LIGO laboratory, 2010.
[101] A. Viterbi, IEEE Trans. Inf. Theory **13**, 260 (1967).
[102] N. Siemonsen, T. May, and W. E. East, Phys. Rev. D **107**, 104003 (2023).
[103] LIGO Scientific, Virgo, and KAGRA Collaborations, LVK Algorithm Library-LALSuite, Free software (GPL) (2018).
[104] K. Wette, SoftwareX **12**, 100634 (2020).
[105] L. Sun, A. Melatos, S. Suvorova, W. Moran, and R. J. Evans, Phys. Rev. D **97**, 043013 (2018).
[106] E. Capote *et al.*, Phys. Rev. D **111**, 062002 (2025).
[107] S. Soni *et al.*, Classical Quantum Gravity **42**, 085016 (2025).
[108] D. Ganapathy *et al.* (LIGO O4 Detector Collaboration), Phys. Rev. X **13**, 041021 (2023).
[109] W. Jia *et al.*, Science **385**, 1318 (2024).
[110] E. Goetz and K. Riles, Segments used for creating standard SFTs in O4 data, Technical Report, LIGO-T2400058 LIGO laboratory, 2024.
[111] D. Davis, A. Neunzert, E. Goetz, K. Riles, K. Wette, and M. Lalleman, Self-gating of O4a h(t) for use in continuous-wave searches, Technical Report, LIGO-T2400003 LIGO Laboratory, 2025.
[112] LIGO Scientific, Virgo, and KAGRA Collaborations, LIGO Virgo KAGRA Calibration Uncertainty (O4), Technical Report, LIGO-T2500288 (LIGO laboratory, 2025), https://dcc.ligo.org/LIGO-T2500288/public.
[113] M. Wade *et al.*, Classical Quantum Gravity **42**, 215016 (2025).
[114] L. Sun *et al.*, Classical Quantum Gravity **37**, 225008 (2020).
[115] A. Viets *et al.*, Classical Quantum Gravity **35**, 095015 (2018).
[116] A. D. Viets, Optimizing advanced LIGO's scientific output with fast, accurate, clean calibration, Ph.D. thesis, University of Wisconsin-Milwaukee, Milwaukee, WI, 2019.
[117] G. Vajente, Y. Huang, M. Isi, J. C. Driggers, J. S. Kissel, M. J. Szczepańczyk, and S. Vitale, Phys. Rev. D **101**, 042003 (2020).
[118] A. G. Abac *et al.* (LIGO Scientific, Virgo, and KAGRA Collaborations), arXiv:2605.27090.
[119] D. Jones and L. Sun, Phys. Rev. D **103**, 023020 (2021).
[120] E. Goetz *et al.*, O4abc.1 lines and combs in found in self-gated C00 cleaned data, Technical Report LIGO-T2600045 (LIGO laboratory, 2026). https://dcc.ligo.org/LIGO-T2600045/public.
[121] E. Goetz *et al.*, arXiv:2606.05959.
[122] A. G. Abac *et al.* (LIGO Scientific, Virgo, and KAGRA Collaborations), Constraints on ultralight bosons from merging binary and remnant black holes observed during the second and third parts of the fourth LIGO-Virgo-KAGRA observing run, (2026) https://dcc.ligo.org/LIGO-P2600218/public.
[123] N. L. Johnson, A. W. Kemp, and S. Kotz, *Univariate Discrete Distributions* (John Wiley & Sons, Ltd., New York, 2005).
[124] S. F. Portegies Zwart and S. McMillan, Astrophys. J. Lett. **528**, L17 (2000).
[125] M. Dominik, K. Belczynski, C. Fryer, D. E. Holz, E. Berti, T. Bulik, I. Mandel, and R. O'Shaughnessy, Astrophys. J. **779**, 72 (2013).
[126] S. S. Bavera, T. Fragos, Y. Qin, E. Zapartas, C. J. Neijssel, I. Mandel, A. Batta, S. M. Gaebel, C. Kimball, and S. Stevenson, Astron. Astrophys. **635**, A97 (2020).
[127] https://dcc.ligo.org/LIGO-M2300033/public.

A. G. Abac,[1] A. Abe,[2] I. Abouelfettouh,[3] F. Acernese,[4,5] K. Ackley,[6] A. Adam,[7] S. Adhicary,[8] D. Adhikari,[9,10] R. X. Adhikari,[11] V. K. Adkins,[12] S. Afroz,[13] A. Agapito,[14] D. Agarwal,[15] M. Agathos,[16] N. Aggarwal,[17] S. Aggarwal,[18] O. D. Aguiar,[19] I.-L. Ahrend,[20] L. Aiello,[21,22] A. Ain,[23] P. Ajith,[24] T. Akutsu,[25,26] L. Albers,[27] W. Ali,[28,29] S. Al-Kershi,[9,10] C. Allene,[30] A. Allocca,[31,5] S. Al-Shammari,[32] J. A. Alvarez,[33] S. Alvarez-Lopez,[34] W. Amar,[35] O. Amarasinghe,[32] A. Amato,[36,37] F. Amicucci,[38,39] C. Amra,[40] A. B. Anand,[33] C. Anand,[41] A. Ananyeva,[11] S. B. Anderson,[11] W. G. Anderson,[11] M. Andia,[42] M. Ando,[43,44] F. Andrade-Oliveira,[45] M. Andrés-Carcasona,[34] J. L. Andrey,[46] T. Andrić,[47,48] J. Anglin,[49] J. Anna,[50] J. M. Antelis,[51] S. Antier,[42] T. Aoki,[52] M. Aoumi,[53] E. Z. Appavuravther,[9,10] E. A. Appelt,[54] S. Appert,[11] S. K. Apple,[55] K. Arai,[11] A. Araya,[56] M. C. Araya,[11] F. Arciprete,[21,22] J. S. Areeda,[57] N. Aritomi,[58] F. Armato,[28,29] S. Armstrong,[59] N. Arnaud,[60] M. Arogeti,[61] S. M. Aronson,[49] K. G. Arun,[62] G. Ashton,[63] Y. Aso,[53,64] L. Asprea,[65] M. Assiduo,[66,67] S. Assis de Souza Melo,[68] S. M. Aston,[69] P. Astone,[38] P. S. Aswathi,[70] F. Attadio,[39,38] F. Aubin,[71] K. AultONeal,[50]

G. Avallone,[4] N. Avdeev,[65] E. A. Avila,[51] S. Babak,[20] C. Badger,[72] S. Bae,[73] S. Bagnasco,[65] S. Baimukhametova,[74,75] L. Baiotti,[76] T. Baka,[77,37] K. A. Baker,[7] T. Baker,[78] G. Balbi,[79] G. Baldi,[80,81] N. Baldicchi,[82,83] M. Ball,[84] G. Ballardin,[68] M. Ballelli,[47,48] S. W. Ballmer,[85] S. Banagiri,[41] B. Banerjee,[47] D. Bankar,[86] T. M. Baptiste,[12] P. Baral,[87] M. Baratti,[88,89] J. C. Barayoga,[11] K. Baric,[11] B. C. Barish,[11] D. Barker,[3] N. Barman,[86] F. Barone,[90,5] B. Barr,[91] M. Barrios,[33] L. Barsotti,[34] M. Barsuglia,[20] D. Barta,[92] M. A. Barton,[91] I. Bartos,[49] A. Basalaev,[9,10] R. Bassiri,[93] A. Basti,[89,88] M. Bawaj,[82,83] J. C. Bayley,[91] A. C. Baylor,[87] P. A. Baynard II,[61] M. Bazzan,[94,95] V. M. Bedakihale,[96] F. Beirnaert,[97] M. Bejger,[98] A. S. Bell,[91] C. Bellani,[99] D. S. Bellie,[100] D. Beltran-Martinez,[101] E. Benedetti,[38] W. Benoit,[18] I. Bentara,[60] M. Ben Yaala,[59] S. Bera,[102] F. Bergamin,[32] B. K. Berger,[93] M. Beroiz,[11] I. Berry,[103] D. Bersanetti,[28] T. Bertheas,[104] A. Bertolini,[37,36] J. Betzwieser,[69] D. Beveridge,[7] N. Bevins,[105] J. Bezerra-Sobrinho,[106] R. Bhandare,[107] R. Bhatt,[11] A. Bhattacharjee,[108] D. Bhattacharjee,[109,110] S. Bhattacharyya,[111] S. Bhaumik,[112] V. Biancalana,[113] F. Bianchi,[83] I. A. Bilenko,[114] M. Bilicki,[115] G. Billingsley,[11] A. Binetti,[99] S. Bini,[11] S. Biot,[116] O. Birnholtz,[117] S. Biscoveanu,[118] A. Bisht,[10] M. Bitossi,[68,88] M.-A. Bizouard,[119] S. Blaber,[120] J. K. Blackburn,[11] L. A. Blagg,[121] C. D. Blair,[7,69] D. G. Blair,[7] M. Bloch,[122] N. Bode,[9,10] N. Boettner,[27] P. Bogdan,[123] G. Boileau,[119] M. Boldrini,[68] G. N. Bolingbroke,[124] L. D. Bonavena,[49] V. A. Bonhomme,[34] E. Bonilla,[93] M. S. Bonilla,[57] A. Bonino,[84] R. Bonnand,[35,125] A. Borchers,[9,10] N. Borghi,[126,79] V. Boschi,[88] S. Bose,[127] V. Bossilkov,[69] Y. Bothra,[37,128] A. Boudon,[60] T. D. Boybeyi,[18] M. Boyle,[129] A. Bozzi,[68] C. Bradaschia,[88] M. J. Brady,[130] P. R. Brady,[87] A. Branch,[69] M. Branchesi,[47,48] T. Briant,[131] A. Brillet,[119,a] M. Brinkmann,[9,10] P. Brockill,[87] E. Brockmueller,[9,10] A. F. Brooks,[11] D. D. Brown,[124] M. L. Brozzetti,[82,83] S. Brunett,[11] G. Bruno,[15] R. Bruntz,[123] J. Bryant,[132] Y. Bu,[133] F. Bucci,[67] A. Buchicchio,[39] A. Buggiani,[68] O. Bulashenko,[134,135] T. Bulik,[136] H. J. Bulten,[37] A. Buonanno,[137,1] K. Burtnyk,[3] R. Buscicchio,[138,139] N. Busdon,[94] D. Buskulic,[35] R. L. Byer,[93] R. Cabrita,[15] V. A. Cáceres-Barbosa,[8] L. Cadonati,[61] G. Cagnoli,[94] C. Cahillane,[85] A. Calafat,[84] J. Calderón Bustillo,[140] J. D. Callaghan,[91] T. A. Callister,[141] E. Calloni,[31,5] S. R. Callos,[121] K. Cannon,[44] V. Cantory,[18] H. Cao,[34] L. A. Capistran,[142] E. Capocasa,[20] G. Capoccia,[83] E. Capote,[3] C. Capuano,[85] G. Capurri,[89,88] F. Carbognani,[68] K. J. Cardona-Martínez,[12] M. Carlassara,[9,10] M. Carpinelli,[138,68] G. Carrillo,[121] G. Carullo,[132] A. Casallas-Lagos,[143] J. Casanueva Diaz,[68] C. Casentini,[144,22] S. Caudill,[145] M. Cavaglià,[110] R. Cavalieri,[68] A. Ceja,[100] G. Cella,[88] P. Cerdá-Durán,[146,147] E. Cesarini,[22] N. Chabbra,[70] W. Chaibi,[119] A. Chakraborty,[13] P. Chakraborty,[9,10] S. Chakraborty,[107] S. Chalathadka Subrahmanya,[27] C. Chan,[148] J. C. L. Chan,[149] M. Chan,[120] C.-Y. Chang,[150] K. Chang,[151] S. Chao,[151] P. Charlton,[152] E. Chassande-Mottin,[20] C. Chatterjee,[54] Debarati Chatterjee,[86] Deep Chatterjee,[34] M. Chaturvedi,[107] S. Chaty,[20] A. Chen,[153] A. H.-Y. Chen,[154] D. Chen,[155] H. Chen,[150] H. Y. Chen,[156] S. Chen,[54] Yanbei Chen,[157] Yiwen Chen,[18] G. Cheng,[153] H. P. Cheng,[103] P. Chessa,[82,83] T. Cheunchitra,[133] H. T. Cheung,[158] S. Y. Cheung,[41] F. Chiadini,[159,160] G. Chiarini,[9,10] A. Chiba,[161] A. Chincarini,[28] D. Chintala,[109] A. Chiummo,[5,68] A. Chopra,[47] C. Chou,[162] S. Choudhary,[7] N. Christensen,[119,163] Y. K. Chu,[87] S. S. Y. Chua,[70] G. Ciani,[80,81] P. Ciecielag,[98] M. Cieślar,[136] M. Cifaldi,[22] B. Cirok,[164] F. Clara,[3] J. A. Clark,[11,61] T. A. Clarke,[118] A. Claveus,[165] M. R. Claypool,[121] S. Clesse,[116] F. Cleva,[119] S. M. Clyne,[130] E. Coccia,[47,48,166] E. Codazzo,[167] P.-F. Cohadon,[131] D. E. Cohen,[9,10] E. Colangeli,[78] O. Cole,[148] M. Colleoni,[84] C. G. Collette,[168] J. Collins,[69] S. Colloms,[91] A. Colombo,[38,169] G. Compère,[116] C. M. Compton,[3] G. Connolly,[121] L. Conti,[95] T. R. Corbitt,[12] I. Cordero-Carrión,[170] S. Corezzi,[82,83] N. J. Cornish,[171] A. Corsi,[172] S. Cortese,[68] L. A. Corubolo,[21,22] L. Cotnoir,[123] R. Cottingham,[69] J. A. Cotturone,[100] M. W. Coughlin,[18] P. Couvares,[11,61] R. Coyne,[130] A. Cozzumbo,[47] J. D. E. Creighton,[87] T. D. Creighton,[173] S. Crook,[69] R. Crouch,[3] J. Csizmazia,[3] K. Csukás,[92] T. J. Cullen,[11] A. Cumming,[91] E. Cuoco,[126,79] M. Cusinato,[146] R. R. Cuzinatto,[174] L. V. da Conceição,[175] T. Dal Canton,[42] S. Dall'Osso,[79,126] S. Dal Pra,[176] G. Dálya,[104] Y. Dang,[8] B. D'Angelo,[28] S. Danilishin,[36,37] O. Danner,[108] S. D'Antonio,[38] K. Danzmann,[9,10] K. E. Darroch,[123] L. P. Dartez,[69] R. Das,[111] S. Das,[86] A. Dasgupta,[96] V. Dattilo,[68] A. Daumas,[20] I. Dave,[107] A. Davenport,[177] T. F. Davies,[7] D. Davis,[130] M. C. Davis,[18] P. Davis,[178,179] E. J. Daw,[180] M. Dax,[1] J. De Bolle,[97] E. deBruin,[18] M. Deenadayalan,[86] J. Degallaix,[181] M. De Laurentis,[31,5] C. J. Delgado Mendez,[101] F. De Lillo,[23] S. Della Torre,[139] W. Del Pozzo,[89,88] O. M. del Rio,[182] A. Demagny,[35] F. De Marco,[39,38] G. Demasi,[183,67] F. De Matteis,[21,22] C. de Melo,[174] N. Demos,[34] T. Dent,[140] A. Depasse,[15] N. DePergola,[105] R. De Pietri,[184,185] R. De Rosa,[31,5] C. De Rossi,[68] E. K. Derrick,[186] M. Desai,[34] D. DeSantis,[34] S. Deshmukh,[54] V. Deshmukh,[91] R. De Simone,[159,160] S. Determan,[187] S. Dhage,[15] A. Dhani,[1] R. Dhatri,[46] R. Dhurkunde,[78] R. Diab,[49] C. Diaz,[101] M. C. Díaz,[173] F. Diaz Guerra,[188,189]

M. Di Cesare,[31,5] M. A. Dicorato,[83,190] T. Dietrich,[1] C. Di Fronzo,[7] M. Di Giovanni,[191,88] D. Diksha,[37,36] J. Ding,[20,192] S. Di Pace,[39,38] I. Di Palma,[39,38] D. Di Piero,[188,189] F. Di Renzo,[67,183] Divyajyoti,[32] A. Dmitriev,[132] J. P. Docherty,[91] Z. Doctor,[100] N. Doerksen,[175] E. Dohmen,[3] A. Doke,[145] A. Domiciano De Souza,[193] L. D'Onofrio,[5] F. Donovan,[34] K. L. Dooley,[32] S. Doravari,[86] O. Dorosh,[194] S. Doshi,[61] F. Dosopoulou,[32] M. Drago,[39,38] J. C. Driggers,[3] M. Dubois,[104] R. S. Dumbreck,[32] U. Dupletsa,[47] D. D'Urso,[195,167] P. Dutta Roy,[49] H. Duval,[196] S. Dwivedi,[197] S. E. Dwyer,[3] C. Eassa,[3] W. E. East,[198] M. Eberhardt,[187] M. Ebersold,[45] M. Ebiri,[199] G. Eddolls,[85] A. Effler,[69] J. Eichholz,[132] H. Einsle,[119] M. Eisenmann,[25] M. Emma,[63] K. Endo,[161] R. Enficiaud,[1] V. Ernst,[15,200] L. Errico,[31,5] R. Espinosa,[173] M. Esposito,[5,31] R. C. Essick,[201] H. Estellés,[84] T. Etzel,[11] M. Evans,[34] T. Evstafyeva,[198] J. M. Ezquiaga,[149] F. Fabrizi,[66,67] V. Fafone,[21,22] S. Fairhurst,[32] X. Fan,[153] A. M. Farah,[201] B. Farr,[121] W. M. Farr,[202,203] M. Favata,[204] M. Fays,[200] M. Fazio,[59] J. Feicht,[11] M. M. Fejer,[93] J.-N. Feldhusen,[27] E. Fenyvesi,[92,205] A. Feo,[184,185] J. Fernandes,[112] T. Fernandes,[206,146] G. Fernández Rodríguez,[170] D. Fernando,[199] S. Ferraiuolo,[207,39,38] T. A. Ferreira,[19] M. Ferrer-Martinez,[84] F. Fidecaro,[89,88] P. Figura,[98] I. Fiori,[68] M. Fishbach,[201] R. P. Fisher,[123] S. K. Fitzgerald,[91] V. Fiumara,[208,160] R. Flaminio,[35] B. Flanagan,[32] S. M. Fleischer,[182] L. S. Fleming,[209] F. Flocco,[94] E. Floden,[18] H. Fong,[120] J. A. Font,[146,147] F. Fontinele-Nunes,[18] C. Foo,[1] B. Fornal,[210] P. W. F. Forsyth,[70] A. Fragkos,[211,75] N. Franchini,[212] A. Franco-Ordovas,[11] F. Frappez,[35] F. Frasconi,[88] C. Fratta,[61] J. P. Freed,[50] Z. Frei,[213] A. Freise,[37,128] O. Freitas,[206,146] R. Frey,[121] W. Frischhertz,[69] P. Fritschel,[34] V. V. Frolov,[69] M. Fuentes-Garcia,[11] R. Fujii,[161] T. Fujimori,[2] Y. Fujiwara,[214] P. Fulda,[49] M. Fyffe,[69] J. R. Gair,[1] S. Galaudage,[193] V. Galdi,[215] M. Galimberti,[68] A. Gamboa,[1] S. Gamoji,[216] A. Ganguly,[86] B. Garaventa,[28] P. García Abia,[101] J. García-Bellido,[217] C. García-Quirós,[84] J. W. Gardner,[70] S. Garg,[44] J. Gargiulo,[68] X. Garrido,[42] A. Garron,[84] F. Garufi,[31,5] P. A. Garver,[93] C. Gasbarra,[218,22] F. Gautier,[219] V. Gayathri,[87] T. Gayer,[85] G. Gemme,[28] A. Gennai,[88] V. Gennari,[104] J. George,[107] R. George,[156] O. Gerberding,[27] L. Gergely,[164] A. Ghinassi,[126,79] Archisman Ghosh,[97] Sayantan Ghosh,[112] Shaon Ghosh,[204] Shrobana Ghosh,[9,10] Suprovo Ghosh,[220] Tathagata Ghosh,[86,221] J. A. Giaime,[12,69] K. D. Giardina,[69] D. R. Gibson,[209] C. Gier,[59] F. Gittins,[77] J. Glanzer,[11] F. Glotin,[42] E. Glowacki,[222] J. Godfrey,[121] R. V. Godley,[9,10] O. Godwin,[11] A. S. Goettel,[223] E. Goetz,[120] J. Golomb,[11] S. Gomez Lopez,[39,38] G. González,[12] P. Goodarzi,[46] S. R. Goode,[41] A. Goodwin-Jones,[15] M. Gosselin,[68] S. M. Goss-Grubbs,[18] C. Gostiaux,[71] R. Gouaty,[35] D. W. Gould,[70] D. Goupilliere,[179,178] K. Govorkova,[34] A. Grado,[82,83] V. Graham,[91] A. E. Granados,[18] M. Granata,[181] V. Granata,[224,160] S. Gras,[34] P. Grassia,[11] C. Gray,[3] R. Gray,[91] G. Greco,[83] A. C. Green,[37,36] L. Green,[225] S. R. Green,[223] A. M. Gretarsson,[50] E. M. Gretarsson,[50] D. Griffith,[11] H. L. Griggs,[61] C. Grimaud,[35] H. Grote,[32] S. Grunewald,[1] A. G. Guerrero,[226] G. M. Guidi,[66,67] T. Guidry,[3] H. K. Gulati,[96] F. Gulminelli,[178,179] H. Guo,[153] W. Guo,[7] Y. Guo,[37] A. Gupta,[227] I. Gupta,[100] N. C. Gupta,[96] S. K. Gupta,[49] V. Gupta,[18] N. Gupte,[1] N. Guttman,[41] F. Guzman,[142] M. Haberland,[1] S. Haino,[228] E. D. Hall,[34] E. Z. Hamilton,[84] G. Hammond,[91] W.-B. Han,[229] M. Haney,[37] J. Hanks,[3] C. Hanna,[8] M. D. Hannam,[32] O. A. Hannuksela,[230] H. Hansen,[3] J. Hanson,[69] R. Harada,[44] A. R. Hardison,[187] S. Harikumar,[98] K. Haris,[231] I. Harley-Trochimczyk,[142] J. Harms,[47,48] G. M. Harry,[232] I. W. Harry,[78] M. T. Hartman,[40,233,20] B. Haskell,[234,235] C.-J. Haster,[225] K. Haughian,[91] H. Hayakawa,[53] K. Hayama,[236] J. Hedberg,[50] A. Heffernan,[84] D. Hegde,[15] M. C. Heintze,[69] J. Heinzel,[34] H. Heitmann,[119] F. Hellman,[33] A. F. Helmling-Cornell,[186] G. Hemming,[68] O. Henderson-Sapir,[124] M. Hendry,[91] I. S. Heng,[91] M. H. Hennig,[91] C. Henshaw,[61] A. Heranval,[8] M. Heurs,[9,10] A. L. Hewitt,[237,238] J. Heynen,[15] J. Heyns,[34] S. Hido,[221] S. Hild,[36,37] M. Hill,[123] S. Hill,[91] Y. Himemoto,[239] C. Hirose,[53] D. Hofman,[181] N. A. Holland,[11] K. Holley-Bockelmann,[54] I. J. Hollows,[180] D. E. Holz,[226] L. Honet,[116] K. M. Hoops,[216] M. E. Hoque,[240] D. J. Horton-Bailey,[33] J. Hough,[91] S. Hourihane,[11] N. T. Howard,[54] E. J. Howell,[7] C. G. Hoy,[78] P. Hsi,[34] H.-Y. Hsieh,[241] C. Hsiung,[242] S.-H. Hsu,[243] W.-F. Hsu,[99] H. Y. Huang,[151] Y. Huang,[8] A. D. Huddart,[244] B. Hughey,[50] D. C. Y. Hui,[245] K. Humphrey,[61] S. Husa,[84] L. Iampieri,[39,38] G. A. Iandolo,[36] M. Ianni,[22,21] Y. Ichinose,[221] K. Ide,[214] R. Iden,[246] A. Ierardi,[47,48] S. Ikeda,[155] H. Imafuku,[44] K. Imai,[221] Y. Inoue,[151] P. Iosif,[188,189] J. Irwin,[91,77] K. Ishida,[2] R. Ishikawa,[214] T. Ishikawa,[52] H. Ishino,[2] M. Isi,[247,203] K. S. Isleif,[248] Y. Itoh,[2,249] S. Iwaguchi,[52] M. M. Iwaya,[32,221] B. R. Iyer,[24] C. Jacquet,[104] T. Jacquot,[42] S. J. Jadhav,[250] S. P. Jadhav,[148] K. Jain,[32] A. L. James,[11] K. Jani,[54] S. Jani,[18] J. Janquart,[15,251] N. N. Janthalur,[250] S. Jaraba,[252] P. Jaranowski,[222] R. Jaume,[84] W. Javed,[32] M. Jensen,[3] W. Jia,[34] J. Jiang,[103] H.-B. Jin,[253,254] S.-J. Jin,[7] G. R. Johns,[123] N. A. Johnson,[49] M. C. Johnston,[225] R. Johnston,[91] N. Johny,[9,10] D. H. Jones,[70] D. I. Jones,[220] R. Jones,[91] P. Joshi,[61] S. K. Joshi,[86] G. Joubert,[60] J. Ju,[255] L. Ju,[7] I. L. Juarez-Reyes,[121] K. Jung,[256] H. B. Kabagoz,[34] B. Kacskovics,[92] T. Kajita,[221]

I. Kaku,[2] V. Kalogera,[100] M. Kalomenopoulos,[225] M. Kamiizumi,[53] N. Kanda,[249,2] S. Kandhasamy,[86] G. Kang,[257] J. B. Kanner,[11] S. J. Kapadia,[86] D. P. Kapasi,[57] A. Karia,[37,128] A. S. Karia,[258] R. Kashyap,[112] M. Kasprzack,[11] H. Kato,[161] T. Kato,[221] E. Katsavounidis,[34] W. Katzman,[69] R. Kaushik,[107] K. Kawabe,[3] S. Kawamura,[52] D. Keitel,[84] S. A. Kemper,[55] L. J. Kemperman,[124] J. Kennington,[8] R. Kesharwani,[86] J. S. Key,[259] R. Khadela,[9,10] S. S. Khadkikar,[8] F. Y. Khalili,[114] C. Khamar,[201] F. Khan,[9,10] M. Khursheed,[107] N. M. Khusid,[202,203] W. Kiendrebeogo,[260] C. Kim,[261] G. Kim,[262] J. C. Kim,[263] K. Kim,[264] M. H. Kim,[255] S. Kim,[245] Y.-M. Kim,[264] C. Kimball,[100] K. Kimes,[57] M. Kinnear,[32] J. S. Kissel,[3] S. Klimenko,[49] A. M. Knee,[158] N. Knust,[9,10] K. Kobayashi,[221] S. M. Koehlenbeck,[93] K. Kohri,[265] K. Kokeyama,[32,52] S. Koley,[47,200] P. Kolitsidou,[84] A. E. Koloniari,[266] K. Komori,[25,43] K. Kompanets,[18] A. K. H. Kong,[267] A. Kontos,[186] K. Kopczuk,[109] L. M. Koponen,[132] M. Korobko,[27] X. Kou,[18] N. Kouvatsos,[72] T. Koyama,[161] D. B. Kozak,[11] E. Kraja,[68] S. L. Kranzhoff,[36,37] V. Kringel,[9,10] N. V. Krishnendu,[132] S. Kroker,[268] A. Królak,[269,194] K. Kruska,[9,10] J. Kubisz,[270] K. Kubota,[221] G. Kuehn,[9,10] D. Kukla,[18] A. Kulur Ramamohan,[70] Achal Kumar,[49] Anil Kumar,[250] Dhruv Kumar,[8,91] Praveen Kumar,[140] Prayush Kumar,[24] Rahul Kumar,[3] Rakesh Kumar,[96] Ravi Kumar,[18] J. Kume,[271,44] K. Kuns,[34] N. Kuntimaddi,[32] S. Kuroyanagi,[217,272] K. Kwak,[256] K. Kwan,[70] S. Kwon,[44] G. Lacaille,[91] D. Laghi,[45] A. H. Laity,[130] N. Lajili,[125,273] A. Lakhal,[131] E. Lalande,[274] M. Lalleman,[23] S. Lalvani,[100] M. Landry,[3] R. N. Lang,[34] A. Lange,[18] J. A. Lange,[65] R. Langgin,[225] B. Lantz,[93] I. La Rosa,[84] O. Laske,[8] P. D. Lasky,[41] L. Lavezzi,[65] J. Lawrence,[173] M. Laxen,[69] A. Lazzarini,[11] C. Lazzaro,[275,167] P. Leaci,[39,38] L. Leali,[18] Y. K. Lecoeuche,[120] H. W. Lee,[276] J. Lee,[85] K. Lee,[255] R.-K. Lee,[150] R. Lee,[34] Sungho Lee,[277] Sunjae Lee,[255] W. Lee,[256] Y. Lee,[151] F. Legger,[65] I. N. Legred,[11] J. Lehmann,[9,10] L. Lehner,[198] M. Le Jean,[181,125] A. Lemaître,[278] R. Lemrani Alaoui,[125,273] M. Lenti,[67,183] M. Leonardi,[80,81,279] M. Lequime,[40] M. Lesovsky,[11] N. Letendre,[35] M. Lethuillier,[60] Y. Levin,[41] S. Lexmond,[128] K. Leyde,[202,203] A. K. Y. Li,[44] K. L. Li,[280] T. G. F. Li,[99] X. Li,[157] Y. Li,[100] Z. Li,[91] Q. Liang,[153] C-Y. Lin,[281] E. T. Lin,[282] F. Lin,[151] L. C.-C. Lin,[280] Y.-C. Lin,[282] C. Lindsay,[209] S. D. Linker,[216] A. Liu,[230] F. Liu,[42] G. C. Liu,[242] Jian Liu,[7] S. Liu,[153] F. Llamas Villarreal,[173] J. Llobera-Querol,[84] R. K. L. Lo,[149] J.-P. Locquet,[99] S. C. G. Loggins,[165] L. T. London,[72] A. Longo,[66,67] M. Lopez Portilla,[77] A. Lorenzo-Medina,[140] V. Loriette,[42] M. Lormand,[69] M. Lorusso,[79] G. Losurdo,[191,88] T. P. Lott IV,[230] J. D. Lough,[9,10] H. A. Loughlin,[34] C. O. Lousto,[199] N. K. Y. Low,[133] N. Lu,[70] H. Lück,[9,10] O. Lukina,[34] D. Lumaca,[22] A. P. Lundgren,[283,166] L. Lunghini,[68] A. W. Lussier,[274] L.-T. Ma,[282] X. Ma,[46] M. Ma'arif,[151] S. MacBride,[45] K. Machida,[161] K. J. Mack,[61] D. M. Macleod,[32] I. A. O. MacMillan,[11] A. Macquet,[42] S. S. Madekar,[166] S. Maenaut,[99] S. S. Magare,[86] R. M. Magee,[11] E. Maggio,[1,38] M. Magnozzi,[28,29] P. Mahapatra,[32] M. Mahesh,[27] S. Majhi,[86] E. Majorana,[39,38] C. N. Makarem,[11] E. Makelele,[109] N. Malagon,[199] D. Malakar,[110] J. A. Malaquias-Reis,[19] U. Mali,[201] S. Maliakal,[11] A. Malik,[107] L. Mallick,[175,201] A.-K. Malz,[63] N. Man,[119] M. Mancarella,[102] V. Mandic,[18] V. Mangano,[195,167] Z. Mangi,[199] B. Mannix,[121] G. L. Mansell,[85] M. Manske,[87] M. Mantovani,[68] M. Mapelli,[94,95,284] S. Marchetti,[94,95] F. Marion,[35] J. Mark,[18] A. S. Markosyan,[93] J. Markus,[18] E. Maros,[11] S. Marsat,[104] F. Martelli,[66,67] I. W. Martin,[91] R. M. Martin,[204] B. B. Martinez,[142] M. Martinez,[166,285] V. Martinez,[286] A. Martini,[80,81] Juan Carlos Martins,[287] Julio C. Martins,[19] D. V. Martynov,[132] E. J. Marx,[34] L. Massaro,[36,37] A. Masserot,[35] M. Masso-Reid,[91] T. Masters,[109] S. Mastrogiovanni,[38] G. Mastropasqua,[79] M. Matiushechkina,[9,10] A. Matte-Landry,[274] L. Maurin,[219] N. Mavalvala,[34] N. Maxwell,[3] A. McCann,[121] G. McCarrol,[69] R. McCarthy,[3] D. E. McClelland,[70] S. McCormick,[69] L. McCuller,[11] L. I. McDermott,[127] C. McElhenny,[123] G. I. McGhee,[91] K. B. M. McGowan,[54] J. McIver,[120] A. McLeod,[7] I. McMahon,[45] T. McRae,[70] R. McTeague,[91] K. McWhirter,[8] D. Meacher,[87] B. N. Meagher,[85] R. Mechum,[199] L. G. Medeiros,[106] R. M. Mehta,[18] A. Melatos,[133] C. S. Menoni,[177] R. A. Mercer,[87] L. Mereni,[181] K. Merfeld,[121] E. L. Merilh,[69] J. R. Mérou,[84] C. Messick,[87] M. Meyer-Conde,[30] F. Meylahn,[9,10] H. Miao,[288] C. Michel,[181] Y. Michimura,[44] H. Middleton,[132] D. P. Mihaylov,[109] A. L. Miller,[153] S. J. Miller,[11] M. Millhouse,[61] E. Milotti,[188,189] V. Milotti,[94] E. Minakaki,[128] Y. Minenkov,[22] Ll. M. Mir,[166] L. Mirasola,[289] C.-A. Miritescu,[166] A. Mishra,[24] C. Mishra,[111] T. Mishra,[78] A. Mitchell,[93] J. G. Mitchell,[50] O. Mitchem,[121] S. Mitra,[86] V. P. Mitrofanov,[114] K. Mitsuhashi,[25] R. Mittleman,[34] O. Miyakawa,[53] S. Miyoki,[53] G. Mo,[11] L. Mobilia,[66,67] S. R. P. Mohapatra,[11] M. Molina-Ruiz,[33] M. Mondin,[216] M. Montani,[66,67] G. Montefusco,[179] C. J. Moore,[237] D. Moraru,[3] A. More,[86] S. More,[86] C. Moreno,[290] E. A. Moreno,[34] G. Moreno,[3] A. Moreso Serra,[134] C. Morgan,[32] S. Morisaki,[221] S. Moriwaki,[221] Y. Moriwaki,[161] G. Morras,[217] A. Moscatello,[94] M. Mould,[223] B. Mours,[71] C. M. Mow-Lowry,[37,128] L. Muccillo,[183,67] F. Muciaccia,[39,38] Arunava Mukherjee,[240] D. Mukherjee,[132]

Samanwaya Mukherjee,[24] Soma Mukherjee,[173] Subroto Mukherjee,[96] Suvodip Mukherjee,[13] N. Mukund,[34] A. Mullavey,[69] C. L. Mungioli,[7] Y. Murakami,[221] M. Murakoshi,[214] P. G. Murray,[91] D. Nabari,[80,81] S. Nadji,[181] A. Nagar,[65,291] N. Nagarajan,[1] K. Nakagaki,[53] A. Nakamura,[52] K. Nakamura,[25] H. Nakano,[292] M. Nakano,[11] D. Nanadoumgar-Lacroze,[166] D. Nandi,[12] V. Napolano,[68] S. U. Naqvi,[111] P. Narayan,[227] A. Nardecchia,[39,38] I. Nardecchia,[22] T. Narikawa,[221] H. Narola,[77] L. Naticchioni,[38] R. K. Nayak,[293] J. Neeson,[32] L. Negri,[77] A. Nela,[91] C. Nelle,[121] A. Nelson,[142] T. J. N. Nelson,[69] A. Nemmani,[98] A. Neunzert,[3] M. Newell,[16] S. Ng,[57] T. C. K. Ng,[37,77] L.-A. T. Nguyen,[294] T. T. Nguyen,[294] L. Nguyen Quynh,[294] A. B. Nielsen,[295] Y. Nishino,[25,296] A. Nishizawa,[297] S. Nissanke,[298,37] W. Niu,[8] F. Nocera,[68] J. Noller,[299] M. Norman,[32] C. North,[32] J. Novak,[252,300] G. Nurbek,[173] L. K. Nuttall,[78] K. Obayashi,[214] J. Oberling,[3] C. E. Ochoa,[46] C. O'Connor,[85] J. O'Dell,[244] E. Oelker,[34] M. Oertel,[252,300] G. Oganesyan,[47,48] J. J. Oh,[263] T. O'Hanlon,[69] M. Ohashi,[53,30] F. Ohme,[9,10] Y. Okabe,[161] I. Oke,[59] R. Oliveira,[301] R. Omer,[18] N. O'Neill,[85] M. Onishi,[161] K. Oohara,[302,303] P. Ophardt,[248] R. J. Oram,[69] B. O'Reilly,[69] R. O'Shaughnessy,[199] S. Oshino,[53] J. Ostrovska,[132] A. Osumi,[52] I. Ota,[12] G. Othman,[248] M. Otsuka,[25,296] D. J. Ottaway,[124] A. Ouzriat,[60] H. Overmier,[69] B. J. Owen,[108] A. E. Pace,[8] M. A. Page,[25] A. Pai,[112] S. Pal,[293] M. A. Palaia,[88,89] M. Pálfi,[213] C. Palomba,[38] H. Pan,[267] J. Pan,[7] K.-C. Pan,[150,282] P. K. Panda,[250] Shiksha Pandey,[8] Swadha Pandey,[34] P. T. H. Pang,[37,77] F. Pannarale,[39,38] B. C. Pant,[107] F. H. Panther,[7] M. Panzeri,[66,67] F. Paoletti,[88] A. Paoli,[68] A. Paolone,[38,304] A. Papadopoulos,[91] E. E. Papalexakis,[46] L. Papalini,[88,89] G. Papigkiotis,[266] A. Paquis,[42] J. Paras,[61] A. Parisi,[82,83] B.-J. Park,[277] Jihwan Park,[261] Junegyu Park,[262] W. Parker,[69] G. Pascale,[9,10] D. Pascucci,[97] A. Pasqualetti,[68] L. Passenger,[41] D. Passuello,[88] O. Patane,[3] A. V. Patel,[151] L. Pathak,[86] A. Patra,[32] B. Patricelli,[89,88] B. G. Patterson,[32] K. Paul,[111,37] S. Paul,[121] E. Payne,[11] T. Pearce,[32] M. Pedraza,[11] A. Pele,[11] F. E. Peña Arellano,[216] X. Peng,[132] Y. Peng,[61] S. Penn,[85,305] A. Perreca,[47,48] J. Perret,[20] D. Pesios,[266] S. Petracca,[215] C. Petrillo,[82] H. P. Pfeiffer,[1] H. Pham,[69] K. A. Pham,[18] K. S. Phukon,[132] H. Phurailatpam,[230] L. Piccari,[39,38] O. J. Piccinni,[84] M. Pichot,[119] A. Pied,[91] M. Piendibene,[89,88] F. Piergiovanni,[66,67] L. Pierini,[38] G. Pierra,[38] V. Pierro,[306,160] M. Pillas,[307,42] B. Pillon,[50] L. Pinard,[181] I. M. Pinto,[306,160,308,31] M. Pinto,[68] B. J. Piotrzkowski,[87] M. Pirello,[3] A. Pisarski,[222] M. D. Pitkin,[237,91] E. Placidi,[39,38] M. L. Planas,[1] C. Plunkett,[34] R. Poggiani,[89,88] E. Polini,[119] M. Polo,[101] J. Pomper,[88,89] L. Pompili,[223] J. Poon,[230] E. Porcelli,[37] A. S. Porter,[108] E. K. Porter,[20] C. Posnansky,[8] J. Powell,[148] G. S. Prabhu,[86] M. Pracchia,[200] A. K. Prajapati,[96] K. Prasai,[309] R. Prasanna,[250] P. Prasia,[310] G. Pratten,[132] G. Principe,[188,189] G. A. Prodi,[80,81] P. Prosperi,[88] P. Prosposito,[21,22] A. Puecher,[1] J. Pullin,[12] M. Punturo,[83] P. Puppo,[38] M. Pürrer,[130] H. Qi,[16] M. Qiao,[153] J. Qin,[70] G. Quéméner,[179,125] V. Quetschke,[173] P. J. Quinonez,[50] R. Rading,[248] I. Rainho,[146] S. Raja,[107] C. Rajan,[107] B. Rajbhandari,[108] M. R. Raj Sah,[13] K. E. Ramirez,[69] F. A. Ramis Vidal,[84] M. Ramos Arevalo,[173] A. Ramos-Buades,[84] S. Ranjan,[61] M. Ranjbar,[46] K. Ransom,[69] P. Rapagnani,[39,38] B. Ratto,[50] A. Ravichandran,[145] A. Ray,[100] V. Raymond,[32] M. Razzano,[89,88] J. Read,[57] J. Redepenning,[18] J. Regan,[225] T. Regimbau,[35] T. Reichardt,[148] S. Reid,[59] C. Reissel,[34] D. H. Reitze,[11] A. I. Renzini,[45,138,139] B. Revenu,[122,42] A. Revilla-Peña,[134] F. Ricci,[39,38] M. Ricci,[38,39] A. Ricciardone,[89,88] J. Rice,[85] J. W. Richardson,[46] M. L. Richardson,[34] K. Riles,[158] H. K. Riley,[32] A. Riminucci,[66,67] F. Robinet,[42] M. Robinson,[3] A. Rocchi,[22] J. Rodriguez,[85] R. Rodriguez Lopez,[177] L. Rolland,[35] J. G. Rollins,[11] A. E. Romano,[311] R. Romano,[4,5] A. Romero-Rodríguez,[35] I. M. Romero-Shaw,[32] J. H. Romie,[69] S. Ronchini,[8,47,48] T. J. Roocke,[124] T. J. Rosauer,[46] C. A. Rose,[61] D. Rosińska,[136] M. P. Ross,[55] M. Rossello-Sastre,[84] S. Rowan,[91] K. Rowlands,[187] S. K. Roy,[202,203] S. Roy,[15,251] T. RoyChowdhury,[87] D. Rozza,[138,139] P. Ruggi,[68] G. H. Ruiz,[165] E. Ruiz Morales,[312,217] K. Ruiz-Rocha,[54] V. Russ,[182] S. M. S,[231] S. Sachdev,[61] T. Sadecki,[3] F. Safai Tehrani,[38] P. Saffarieh,[37,128] S. Safi-Harb,[175] S. Saha,[282] T. Sainrat,[20] S. Sajith Menon,[313,39,38] K. Sakai,[314] Y. Sakai,[30] M. Sakellariadou,[72] S. Sakon,[8] F. Salces-Carcoba,[11] L. Salconi,[68] M. Saleem,[156] F. Salemi,[39,38] M. Sallé,[37] M. Salomé,[60] S. U. Salunkhe,[86] S. Salvador,[179,178] A. Salvarese,[156] A. Samajdar,[77,37] P. M. Samir,[186] A. Sanchez,[3] E. J. Sanchez,[11] J. Sanchez,[69] D. Sanchez-Cid,[45] N. Sanchis-Gual,[146] J. R. Sanders,[187] E. M. Sänger,[1] F. Santoliquido,[47,48] E. Sapkin,[41] F. Sarandrea,[65] T. R. Saravanan,[86] N. Sarin,[237] P. Sarkar,[9,10] A. Sasli,[18] P. Sassi,[83,82] B. Sassolas,[181] B. S. Sathyaprakash,[8,32] O. Sauter,[49] R. L. Savage,[3] T. Savicheva,[177] T. Sawada,[53] H. L. Sawant,[86] D. Schaetzl,[11] M. Scheel,[157] A. Schiebelbein,[201] M. G. Schiworski,[85] K. Schluterman,[50] P. Schmidt,[132] R. Schnabel,[27] M. Schneewind,[9,10] R. M. S. Schofield,[121,3] M. Schoor,[35] K. Schouteden,[99] B. W. Schulte,[9,10] M. Schulz,[47,48] B. F. Schutz,[32,9,10] E. Schwartz,[197] M. Scialpi,[315] J. Scott,[91] S. M. Scott,[70] R. M. Sedas,[69] T. C. Seetharamu,[91] M. Seglar-Arroyo,[166] Y. Sekiguchi,[316] D. Sellers,[69] N. Sembo,[2] E. G. Seo,[91] J. W. Seo,[99] G. Seong,[261] V. Sequino,[31,5]

M. Serra,[38] C. K. Sethi,[145] A. Sevrin,[196] T. Shaffer,[3] U. S. Shah,[61] M. A. Shaikh,[317] L. Shao,[318] J. Sharkey,[91] A. K. Sharma,[84] Preeti Sharma,[12] Priyanka Sharma,[107] Sushant Sharma-Chaudhary,[18] P. Shawhan,[137] T. Shen,[70] E. Sheridan,[54] Z.-H. Shi,[150] K. Shimode,[53] H. Shinkai,[319] S. Shirke,[86] D. H. Shoemaker,[34] D. M. Shoemaker,[156] R. W. Short,[3] S. ShyamSundar,[107] H. Siegel,[198] N. Siemonsen,[198,118] V. Sierra,[290] D. Sigg,[3] L. Silenzi,[36,37] P. J. S. Silva,[287] L. Silvestri,[39,176] M. Simmonds,[124] L. P. Singer,[320] A. Singh,[227] D. Singh,[33] M. K. Singh,[32] N. Singh,[84] S. Singh,[246,25] M. R. Sinha,[41] A. M. Sintes,[84] V. Skliris,[32] B. J. J. Slagmolen,[70] T. J. Slaven-Blair,[7] J. Smetana,[132] D. A. Smith,[69] J. R. Smith,[57] J. Smith,[32] L. Smith,[188,189] W. J. Smith,[54] S. Soares de Albuquerque Filho,[66,67] M. Soares-Santos,[45] K. Somiya,[246] I. Song,[282] S. Soni,[46] V. Sordini,[60] F. Sorrentino,[28] H. Sotani,[321] N. E. Sovitzky,[322] F. Spada,[88] V. Spagnuolo,[37] A. P. Spencer,[91] M. Spera,[189,323] P. Spinicelli,[68] A. K. Srivastava,[96] F. Stachurski,[91] V. V. Stanford,[108] A. Stanton,[32] D. A. Steer,[324] N. Steinle,[175] J. Steinlechner,[36,37] S. Steinlechner,[36,37] C. Stephens,[32] N. Stergioulas,[266] M. StPierre,[130] J. Stremiz,[57] M. D. Strong,[12] A. Strunk,[3] R. Sturani,[325] M. Suchenek,[98] S. Sudhagar,[98] R. Sugimoto,[43] L. Suleiman,[57] K. D. Sullivan,[12] J. Sun,[263,80] L. Sun,[70] S. Sunil,[96] J. Suresh,[119] P. J. Sutton,[32] K. Suzuki,[246] M. Suzuki,[221] A. Svizzeretto,[82] B. L. Swinkels,[37] A. Syx,[125] M. J. Szczepańczyk,[143] M. Tacca,[37] M. Tagliazucchi,[126,79] H. Tagoshi,[221] S. C. Tait,[11] H. Takaba,[155] K. Takada,[221] H. Takahashi,[30] R. Takahashi,[25] A. Takamori,[56] S. Takano,[9,10] H. Takeda,[326,327] I. Takimoto Schmiegelow,[47,48] C. Talbot,[118] M. Tamaki,[221] N. Tamanini,[104] D. Tanabe,[151] K. Tanaka,[246] S. J. Tanaka,[214] S. Tanioka,[32] D. B. Tanner,[49] W. Tanner,[9,10] L. Tao,[46] R. D. Tapia,[8] E. N. Tapia San Martín,[37] A. Taruya,[328] J. D. Tasson,[163] J. G. Tau,[199] A. Tejera,[172] J. G. Temple,[109] Y. Teng,[87] H. Themann,[216] A. Theodoropoulos,[146] M. P. Thirugnanasambandam,[86] L. M. Thomas,[11] M. Thomas,[69] P. Thomas,[3] J. E. Thompson,[220] S. R. Thondapu,[107] E. Thrane,[41] J. Tissino,[47,48] A. Tiwari,[86] Pawan Tiwari,[47] Praveer Tiwari,[62] S. Tiwari,[45] V. Tiwari,[132] M. R. Todd,[85] E. Tofani,[38] M. Toffano,[94] A. M. Toivonen,[18] K. Toland,[91] T. Tomaru,[25] V. Tommasini,[11] H. Tong,[41] C. I. Torrie,[11] I. Tosta e Melo,[329] E. Tournefier,[35] A. Trapananti,[190,83] R. Travaglini,[79] F. Travasso,[190,83] G. Traylor,[69] L. Traylor,[57] M. Trevor,[137] M. C. Tringali,[68] A. Tripathee,[158] G. Troian,[188,189] A. Trovato,[188,189] L. Trozzo,[5] R. J. Trudeau,[11] T. Tsang,[330] S. Tsuchida,[331] K. Tsuji,[52] L. Tsukada,[225] A. Tuci,[50] M. Turconi,[119] C. Turski,[97] H. Ubach,[134,135] A. S. Ubhi,[132] N. Uchikata,[221] T. Uchiyama,[53] R. P. Udall,[120] T. Uehara,[332] V. Undheim,[295] V. Upadhyaya,[145] L. E. Uronen,[230] T. Ushiba,[53] M. Vacatello,[88,89] H. Vahlbruch,[9,10] G. Vajente,[11] J. Valencia,[84] M. Valentini,[128,37] E. Vallejo-Pagès,[166] S. A. Vallejo-Peña,[311] S. Vallero,[65] M. van Dael,[37,333] E. Van den Bossche,[196] J. F. J. van den Brand,[36,128,37] C. Van Den Broeck,[77,37] M. van der Kolk,[128] M. van der Sluys,[77,37] A. Van de Walle,[42] J. van Dongen,[37] K. Vandra,[105] M. VanDyke,[127] H. van Haevermaet,[23] J. V. van Heijningen,[37] P. Van Hove,[71] J. Vanier,[274] J. Vanosky,[3] N. van Remortel,[23] M. Vardaro,[36,37] A. F. Vargas,[133] V. Varma,[145] A. Vecchio,[132] G. Vedovato,[95] J. Veitch,[91] P. J. Veitch,[124] S. Venikoudis,[15] P. Verdier,[60] M. Vereecken,[97] D. Verkindt,[35] B. Verma,[145] S. Verma,[116] Y. Verma,[107] S. M. Vermeulen,[11] F. Vetrano,[66] A. Veutro,[38,39] A. Viceré,[66,67] S. Vidyant,[85] A. D. Viets,[322] A. Vijaykumar,[201] A. Vilkha,[199] N. Villanueva Espinosa,[146] E. T. Vincent,[61] J.-Y. Vinet,[119] S. Viret,[60] S. Vitale,[34] A. Vives,[121] L. Vizmeg,[182] B. Vizzone,[61] H. Vocca,[82,83] D. Voigt,[27] E. R. G. von Reis,[3] J. S. A. von Wrangel,[9,10] W. E. Vossius,[248] L. Vujeva,[149] S. P. Vyatchanin,[114] J. Wack,[11] L. E. Wade,[109] M. Wade,[109] K. J. Wagner,[199] L. Wallace,[11] R.-Z. Wan,[334] H. Wang,[246] L. Wang,[61] P. Wang,[150] W. H. Wang,[173] Y. F. Wang,[1] Z. Wang,[153] R. L. Ward,[70] J. Warner,[3] M. Was,[35] T. Washimi,[25] N. Y. Washington,[11] D. Watarai,[44] B. Weaver,[3] S. A. Webster,[91] N. L. Weickhardt,[27] M. Weinert,[9,10] A. J. Weinstein,[11] R. Weiss,[34,b] L. Wen,[7] K. Wette,[70] C. Wheeler,[69] J. T. Whelan,[199] B. F. Whiting,[49] E. G. Wickens,[78] D. Wilken,[9,10] B. M. Williams,[127] D. Williams,[91] M. J. Williams,[78] N. S. Williams,[1] J. L. Willis,[11] B. Willke,[9,10] M. Wils,[99] L. Wimmer,[221] C. W. Winborn,[110] A. Wingfield,[123] J. Winterflood,[7] C. C. Wipf,[11] G. Woan,[91] N. E. Wolfe,[34] H. T. Wong,[151] I. C. F. Wong,[99] T. Wouters,[77,37] J. L. Wright,[3] M. Wright,[77] B. Wu,[85] C. Wu,[150] D. S. Wu,[9,10] H. Wu,[150] J. Wu,[61] K. Wu,[127] Z. Wu,[104] E. Wuchner,[57] D. M. Wysocki,[87] V. A. Xu,[33] Y. Xu,[84] N. Yadav,[65] H. Yamamoto,[11] K. Yamamoto,[161] T. S. Yamamoto,[44] T. Yamamoto,[53] R. Yamazaki,[214] T. Yan,[132] H. Yang,[288] K. Z. Yang,[18] Y. Yang,[162] Z. Yarbrough,[12] J. Yébana Carrilero,[84] A. B. Yelikar,[54] X. Yin,[34] J. Yokoyama,[335,44,43] T. Yokozawa,[53] M. Yoshihara,[52] S. Yuan,[7] H. Yuzurihara,[53] M. Zanatta,[80] M. Zanolin,[50] M. Zeeshan,[199] T. Zelenova,[68] J.-P. Zendri,[95] M. Zeoli,[15] M. Zerrad,[40] M. Zevin,[100] H. Zhang,[153] J. Zhang,[15] L. Zhang,[11] N. Zhang,[61] R. Zhang,[103] T. Zhang,[132] C. Zhao,[7] J. Zhao,[336] Yue Zhao,[337] Yuhang Zhao,[20] L.-M. Zheng,[32] Y. Zheng,[110] L. Zhizhong,[83] H. Zhong,[18] H. Zhou,[85] H. O. Zhu,[7] X.-J. Zhu,[336] Z.-H. Zhu,[336,334]

Z. Zhu,[199] D. Z. Zieba,[91] A. B. Zimmerman,[156] L. Zimmermann,[60] and M. E. Zucker[34,11]

(LIGO Scientific Collaboration, Virgo Collaboration, and KAGRA Collaboration)

[1]*Max Planck Institute for Gravitational Physics (Albert Einstein Institute), D-14476 Potsdam, Germany*
[2]*Department of Physics, Graduate School of Science, Osaka Metropolitan University, 3-3-138 Sugimoto-cho, Sumiyoshi-ku, Osaka City, Osaka 558-8585, Japan*
[3]*LIGO Hanford Observatory, Richland, Washington 99352, USA*
[4]*Dipartimento di Fisica "E.R. Caianiello," Università di Salerno, I-84084 Fisciano, Salerno, Italy*
[5]*INFN, Sezione di Napoli, I-80126 Napoli, Italy*
[6]*University of Warwick, Coventry CV4 7AL, United Kingdom*
[7]*OzGrav, University of Western Australia, Crawley, Western Australia 6009, Australia*
[8]*The Pennsylvania State University, University Park, Pennsylvania 16802, USA*
[9]*Max Planck Institute for Gravitational Physics (Albert Einstein Institute), D-30167 Hannover, Germany*
[10]*Leibniz Universität Hannover, D-30167 Hannover, Germany*
[11]*LIGO Laboratory, California Institute of Technology, Pasadena, California 91125, USA*
[12]*Louisiana State University, Baton Rouge, Louisiana 70803, USA*
[13]*Tata Institute of Fundamental Research, Mumbai 400005, India*
[14]*Centre de Physique Théorique, Aix-Marseille Université, Campus de Luminy, 163 Avenue de Luminy, 13009 Marseille, France*
[15]*Université catholique de Louvain, B-1348 Louvain-la-Neuve, Belgium*
[16]*Queen Mary University of London, London E1 4NS, United Kingdom*
[17]*University of California, Davis, Davis, California 95616, USA*
[18]*University of Minnesota, Minneapolis, Minnesota 55455, USA*
[19]*Instituto Nacional de Pesquisas Espaciais, 12227-010 São José dos Campos, São Paulo, Brazil*
[20]*Université Paris Cité, CNRS, Astroparticule et Cosmologie, F-75013 Paris, France*
[21]*Università di Roma Tor Vergata, I-00133 Roma, Italy*
[22]*INFN, Sezione di Roma Tor Vergata, I-00133 Roma, Italy*
[23]*Universiteit Antwerpen, 2000 Antwerpen, Belgium*
[24]*International Centre for Theoretical Sciences, Tata Institute of Fundamental Research, Bengaluru 560089, India*
[25]*Gravitational Wave Science Project, National Astronomical Observatory of Japan, 2-21-1 Osawa, Mitaka City, Tokyo 181-8588, Japan*
[26]*Advanced Technology Center, National Astronomical Observatory of Japan, 2-21-1 Osawa, Mitaka City, Tokyo 181-8588, Japan*
[27]*Universität Hamburg, D-22761 Hamburg, Germany*
[28]*INFN, Sezione di Genova, I-16146 Genova, Italy*
[29]*Dipartimento di Fisica, Università degli Studi di Genova, I-16146 Genova, Italy*
[30]*Research Center for Space Science, Advanced Research Laboratories, Tokyo City University, 3-3-1 Ushikubo-Nishi, Tsuzuki-Ku, Yokohama, Kanagawa 224-8551, Japan*
[31]*Università di Napoli "Federico II," I-80126 Napoli, Italy*
[32]*Cardiff University, Cardiff CF24 3AA, United Kingdom*
[33]*University of California, Berkeley, California 94720, USA*
[34]*LIGO Laboratory, Massachusetts Institute of Technology, Cambridge, Massachusetts 02139, USA*
[35]*Univ. Savoie Mont Blanc, CNRS, Laboratoire d'Annecy de Physique des Particules-IN2P3, F-74000 Annecy, France*
[36]*Maastricht University, 6200 MD Maastricht, Netherlands*
[37]*Nikhef, 1098 XG Amsterdam, Netherlands*
[38]*INFN, Sezione di Roma, I-00185 Roma, Italy*
[39]*Università di Roma "La Sapienza," I-00185 Roma, Italy*
[40]*Aix Marseille Univ, CNRS, Centrale Med, Institut Fresnel, F-13013 Marseille, France*
[41]*OzGrav, School of Physics & Astronomy, Monash University, Clayton 3800, Victoria, Australia*
[42]*Université Paris-Saclay, CNRS/IN2P3, IJCLab, 91405 Orsay, France*
[43]*Department of Physics, The University of Tokyo, 7-3-1 Hongo, Bunkyo-ku, Tokyo 113-0033, Japan*
[44]*Research Center for the Early Universe (RESCEU), The University of Tokyo, 7-3-1 Hongo, Bunkyo-ku, Tokyo 113-0033, Japan*

[45]*University of Zurich, Winterthurerstrasse 190, 8057 Zurich, Switzerland*
[46]*University of California, Riverside, Riverside, California 92521, USA*
[47]*Gran Sasso Science Institute (GSSI), I-67100 L'Aquila, Italy*
[48]*INFN, Laboratori Nazionali del Gran Sasso, I-67100 Assergi, Italy*
[49]*University of Florida, Gainesville, Florida 32611, USA*
[50]*Embry-Riddle Aeronautical University, Prescott, Arizona 86301, USA*
[51]*Tecnologico de Monterrey, Escuela de Ingeniería y Ciencias, 64849 Monterrey, Nuevo León, Mexico*
[52]*Nagoya University, Nagoya, 464-8601, Japan*
[53]*KAGRA Observatory, Institute for Cosmic Ray Research, The University of Tokyo, 238 Higashi-Mozumi, Kamioka-cho, Hida City, Gifu 506-1205, Japan*
[54]*Vanderbilt University, Nashville, Tennessee 37235, USA*
[55]*University of Washington, Seattle, Washington 98195, USA*
[56]*Earthquake Research Institute, The University of Tokyo, 1-1-1 Yayoi, Bunkyo-ku, Tokyo 113-0032, Japan*
[57]*California State University Fullerton, Fullerton, California 92831, USA*
[58]*Department of Applied Physics, Graduate School of Engineering, The University of Tokyo, 7-3-1 Hongo, Bunkyo-ku, Tokyo 113-8656, Japan*
[59]*SUPA, University of Strathclyde, Glasgow G1 1XQ, United Kingdom*
[60]*Université Claude Bernard Lyon 1, CNRS, IP2I Lyon / IN2P3, UMR 5822, F-69622 Villeurbanne, France*
[61]*Georgia Institute of Technology, Atlanta, Georgia 30332, USA*
[62]*Chennai Mathematical Institute, Chennai 603103, India*
[63]*Royal Holloway, University of London, London TW20 0EX, United Kingdom*
[64]*Department of Astronomical Science, The Graduate University for Advanced Studies (SOKENDAI), 2-21-1 Osawa, Mitaka City, Tokyo 181-8588, Japan*
[65]*INFN Sezione di Torino, I-10125 Torino, Italy*
[66]*Università degli Studi di Urbino "Carlo Bo," I-61029 Urbino, Italy*
[67]*INFN, Sezione di Firenze, I-50019 Sesto Fiorentino, Firenze, Italy*
[68]*European Gravitational Observatory (EGO), I-56021 Cascina, Pisa, Italy*
[69]*LIGO Livingston Observatory, Livingston, Louisiana 70754, USA*
[70]*OzGrav, Australian National University, Canberra, Australian Capital Territory 0200, Australia*
[71]*Université de Strasbourg, CNRS, IPHC UMR 7178, F-67000 Strasbourg, France*
[72]*King's College London, University of London, London WC2R 2LS, United Kingdom*
[73]*Korea Institute of Science and Technology Information, Daejeon 34141, Republic of Korea*
[74]*Département de Physique Nucléaire et Corpusculaire, Université de Genève, 24 quai E. Ansermet, CH-1211 Geneva, Switzerland*
[75]*Gravitational Wave Science Center (GWSC), Université de Genève, CH-1211 Geneva, Switzerland*
[76]*International College, The University of Osaka, 1-1 Machikaneyama-cho, Toyonaka City, Osaka 560-0043, Japan*
[77]*Institute for Gravitational and Subatomic Physics (GRASP), Utrecht University, 3584 CC Utrecht, Netherlands*
[78]*University of Portsmouth, Portsmouth, PO1 3FX, United Kingdom*
[79]*Istituto Nazionale Di Fisica Nucleare-Sezione di Bologna, viale Carlo Berti Pichat 6/2–40127 Bologna, Italy*
[80]*Università di Trento, Dipartimento di Fisica, I-38123 Povo, Trento, Italy*
[81]*INFN, Trento Institute for Fundamental Physics and Applications, I-38123 Povo, Trento, Italy*
[82]*Università di Perugia, I-06123 Perugia, Italy*
[83]*INFN, Sezione di Perugia, I-06123 Perugia, Italy*
[84]*IAC3-IEEC, Universitat de les Illes Balears, E-07122 Palma de Mallorca, Spain*
[85]*Syracuse University, Syracuse, New York 13244, USA*
[86]*Inter-University Centre for Astronomy and Astrophysics, Pune 411007, India*
[87]*University of Wisconsin-Milwaukee, Milwaukee, Wisconsin 53201, USA*
[88]*INFN, Sezione di Pisa, I-56127 Pisa, Italy*
[89]*Università di Pisa, I-56127 Pisa, Italy*
[90]*Dipartimento di Medicina, Chirurgia e Odontoiatria "Scuola Medica Salernitana," Università di Salerno, I-84081 Baronissi, Salerno, Italy*
[91]*IGR, University of Glasgow, Glasgow G12 8QQ, United Kingdom*

[92]HUN-REN Wigner Research Centre for Physics, H-1121 Budapest, Hungary
[93]Stanford University, Stanford, California 94305, USA
[94]Università di Padova, Dipartimento di Fisica e Astronomia, I-35131 Padova, Italy
[95]INFN, Sezione di Padova, I-35131 Padova, Italy
[96]Institute for Plasma Research, Bhat, Gandhinagar 382428, India
[97]Universiteit Gent, B-9000 Gent, Belgium
[98]Nicolaus Copernicus Astronomical Center, Polish Academy of Sciences, 00-716, Warsaw, Poland
[99]Katholieke Universiteit Leuven, Oude Markt 13, 3000 Leuven, Belgium
[100]Northwestern University, Evanston, Illinois 60208, USA
[101]Centro de Investigaciones Energéticas Medioambientales y Tecnológicas, Avenida Complutense 40, 28040, Madrid, Spain
[102]Aix-Marseille Université,
Université de Toulon, CNRS, CPT, Marseille, France
[103]Northeastern University, Boston, Massachusetts 02115, USA
[104]Laboratoire des 2 infinis-Toulouse, Université de Toulouse,
CNRS/IN2P3, Toulouse, France
[105]Villanova University,
Villanova, Pennsylvania 19085, USA
[106]Federal University of Rio Grande do Norte,
Campus Universitário-Lagoa Nova, Natal-RN, 59078-970, Brazil
[107]RRCAT, Indore, Madhya Pradesh 452013, India
[108]University of Maryland,
Baltimore County, Baltimore, Maryland 21250, USA
[109]Kenyon College, Gambier, Ohio 43022, USA
[110]Missouri University of Science and Technology, Rolla, Missouri 65409, USA
[111]Indian Institute of Technology Madras, Chennai 600036, India
[112]Indian Institute of Technology Bombay, Powai, Mumbai 400 076, India
[113]Università di Siena, Dipartimento di Scienze Fisiche, della Terra e dell'Ambiente, I-53100 Siena, Italy
[114]Lomonosov Moscow State University, Moscow 119991, Russia
[115]Center for Theoretical Physics, Polish Academy of Sciences, 02-668, Warsaw, Poland
[116]Université libre de Bruxelles, 1050 Bruxelles, Belgium
[117]Bar-Ilan University, Ramat Gan, 5290002, Israel
[118]Princeton University, Princeton, New Jersey 08544, USA
[119]Université Côte d'Azur, Observatoire de la Côte d'Azur, CNRS, Artemis, F-06304 Nice, France
[120]University of British Columbia, Vancouver, British Columbia V6T 1Z4, Canada
[121]University of Oregon, Eugene, Oregon 97403, USA
[122]Subatech, CNRS/IN2P3-IMT Atlantique-Nantes Université, 4 rue Alfred Kastler BP 20722 44307
Nantes CÉDEX 03, France
[123]Christopher Newport University, Newport News, Virginia 23606, USA
[124]OzGrav, University of Adelaide, Adelaide, South Australia 5005, Australia
[125]Centre national de la recherche scientifique, 75016 Paris, France
[126]DIFA-Alma Mater Studiorum Università di Bologna, Via Zamboni, 33–40126 Bologna, Italy
[127]Washington State University,
Pullman, Washington 99164, USA
[128]Department of Physics and Astronomy, Vrije Universiteit Amsterdam,
1081 HV Amsterdam, Netherlands
[129]Cornell University, Ithaca, New York 14850, USA
[130]University of Rhode Island, Kingston, Rhode Island 02881, USA
[131]Laboratoire Kastler Brossel, Sorbonne Université, CNRS, ENS-Université PSL, Collège de France,
F-75005 Paris, France
[132]University of Birmingham, Birmingham B15 2TT, United Kingdom
[133]OzGrav, University of Melbourne, Parkville, Victoria 3010, Australia
[134]Institut de Ciències del Cosmos (ICCUB), Universitat de Barcelona (UB),
c. Martí i Franquès, 1, 08028 Barcelona, Spain
[135]Departament de Física Quàntica i Astrofísica (FQA), Universitat de Barcelona (UB), c. Martí i Franqués, 1, 08028 Barcelona, Spain
[136]Astronomical Observatory, University of Warsaw, 00-478 Warsaw, Poland

[137]*University of Maryland, College Park, Maryland 20742, USA*
[138]*Università degli Studi di Milano-Bicocca, I-20126 Milano, Italy*
[139]*INFN, Sezione di Milano-Bicocca, I-20126 Milano, Italy*
[140]*IGFAE, Universidade de Santiago de Compostela, E-15782 Santiago de Compostela, Spain*
[141]*Williams College, Williamstown, Massachusetts 01267 USA*
[142]*University of Arizona, Tucson, Arizona 85721, USA*
[143]*Faculty of Physics, University of Warsaw, Ludwika Pasteura 5, 02-093 Warszawa, Poland*
[144]*Istituto di Astrofisica e Planetologia Spaziali di Roma, 00133 Roma, Italy*
[145]*University of Massachusetts Dartmouth, North Dartmouth, Massachusetts 02747, USA*
[146]*Departamento de Astronomía y Astrofísica, Universitat de València, E-46100 Burjassot, València, Spain*
[147]*Observatori Astronòmic, Universitat de València, E-46980 Paterna, València, Spain*
[148]*OzGrav, Swinburne University of Technology, Hawthorn VIC 3122, Australia*
[149]*Niels Bohr Institute, University of Copenhagen, 2100 Kóbenhavn, Denmark*
[150]*Department of Physics, National Tsing Hua University, No. 101 Section II, Kuang-Fu Road, Hsinchu 30013, Taiwan*
[151]*National Central University, Taoyuan City 320317, Taiwan*
[152]*OzGrav, Charles Sturt University, Wagga Wagga, New South Wales 2678, Australia*
[153]*University of Chinese Academy of Sciences / International Centre for Theoretical Physics Asia-Pacific, Beijing 100190, China*
[154]*Institute of Physics, National Yang Ming Chiao Tung University, 101 Univ. Street, Hsinchu, Taiwan*
[155]*Kamioka Branch, National Astronomical Observatory of Japan, 238 Higashi-Mozumi, Kamioka-cho, Hida City, Gifu 506-1205, Japan*
[156]*University of Texas, Austin, Texas 78712, USA*
[157]*CaRT, California Institute of Technology, Pasadena, California 91125, USA*
[158]*University of Michigan, Ann Arbor, Michigan 48109, USA*
[159]*Dipartimento di Ingegneria Industriale (DIIN), Università di Salerno, I-84084 Fisciano, Salerno, Italy*
[160]*INFN, Sezione di Napoli, Gruppo Collegato di Salerno, I-80126 Napoli, Italy*
[161]*Faculty of Science, University of Toyama, 3190 Gofuku, Toyama City, Toyama 930-8555, Japan*
[162]*School of Physical Science and Technology, ShanghaiTech University, 393 Middle Huaxia Road, Pudong, Shanghai, 201210, China*
[163]*Carleton College, Northfield, Minnesota 55057, USA*
[164]*University of Szeged, Dóm tér 9, Szeged 6720, Hungary*
[165]*St. Thomas University, Miami Gardens, Florida 33054, USA*
[166]*Institut de Física d'Altes Energies (IFAE), The Barcelona Institute of Science and Technology, Campus UAB, E-08193 Bellaterra (Barcelona), Spain*
[167]*INFN Cagliari, Physics Department, Università degli Studi di Cagliari, Cagliari 09042, Italy*
[168]*Université Libre de Bruxelles, Brussels 1050, Belgium*
[169]*INAF, Osservatorio Astronomico di Brera sede di Merate, I-23807 Merate, Lecco, Italy*
[170]*Departamento de Matemáticas, Universitat de València, E-46100 Burjassot, València, Spain*
[171]*Montana State University, Bozeman, Montana 59717, USA*
[172]*Johns Hopkins University, Baltimore, Maryland 21218, USA*
[173]*The University of Texas Rio Grande Valley, Brownsville, Texas 78520, USA*
[174]*Instituto de Ciências e Tecnologia-Universidade Federal de Alfenas, BR 267-Rodovia José Aurélio Vilela, n° 11.999, Km 533 37715-400 Cidade Universitária-Poços de Caldas-MG-Brasil, Brazil*
[175]*University of Manitoba, Winnipeg, Manitoba R3T 2N2, Canada*
[176]*INFN-CNAF-Bologna, Viale Carlo Berti Pichat, 6/2, 40127 Bologna BO, Italy*
[177]*Colorado State University, Fort Collins, Colorado 80523, USA*
[178]*Université de Normandie, ENSICAEN, UNICAEN, CNRS/IN2P3, LPC Caen, F-14000 Caen, France*
[179]*Laboratoire de Physique Corpusculaire Caen, 6 boulevard du maréchal Juin, F-14050 Caen, France*
[180]*The University of Sheffield, Sheffield S10 2TN, United Kingdom*
[181]*Université Claude Bernard Lyon 1, CNRS, Laboratoire des Matériaux Avancés (LMA), IP2I Lyon / IN2P3, UMR 5822, F-69622 Villeurbanne, France*
[182]*Western Washington University, Bellingham, Washington 98225, USA*
[183]*Università di Firenze, Sesto Fiorentino I-50019, Italy*
[184]*Università di Parma, I-43124 Parma, Italy*
[185]*INFN, Sezione di Milano Bicocca, Gruppo Collegato di Parma, I-43124 Parma, Italy*

[186]Bard College, Annandale-On-Hudson, New York 12504, USA
[187]Marquette University, Milwaukee, Wisconsin 53233, USA
[188]Dipartimento di Fisica, Università di Trieste, I-34127 Trieste, Italy
[189]INFN, Sezione di Trieste, I-34127 Trieste, Italy
[190]Università di Camerino, I-62032 Camerino, Italy
[191]Scuola Normale Superiore, I-56126 Pisa, Italy
[192]Corps des Mines, Mines Paris, Université PSL, 60 Bd Saint-Michel, 75272 Paris, France
[193]Université Côte d'Azur, Observatoire de la Côte d'Azur, CNRS, Lagrange, F-06304 Nice, France
[194]National Center for Nuclear Research, 05-400 Świerk-Otwock, Poland
[195]Università degli Studi di Sassari, I-07100 Sassari, Italy
[196]Vrije Universiteit Brussel, 1050 Brussel, Belgium
[197]Trinity College, Hartford, Connecticut 06106, USA
[198]Perimeter Institute, Waterloo, Ontario N2L 2Y5, Canada
[199]Rochester Institute of Technology, Rochester, New York 14623, USA
[200]Université de Liège, B-4000 Liège, Belgium
[201]Canadian Institute for Theoretical Astrophysics, University of Toronto, Toronto, Ontario M5S 3H8, Canada
[202]Stony Brook University, Stony Brook, New York 11794, USA
[203]Center for Computational Astrophysics, Flatiron Institute, New York, New York 10010, USA
[204]Montclair State University, Montclair, New Jersey 07043, USA
[205]HUN-REN Institute for Nuclear Research, H-4026 Debrecen, Hungary
[206]Centro de Física das Universidades do Minho e do Porto, Universidade do Minho, PT-4710-057 Braga, Portugal
[207]Aix Marseille Univ, CNRS/IN2P3, CPPM, Marseille, France
[208]Dipartimento di Ingegneria, Università della Basilicata, I-85100 Potenza, Italy
[209]SUPA, University of the West of Scotland, Paisley PA1 2BE, United Kingdom
[210]Barry University, Miami Shores, Florida 33168, USA
[211]Department of Astronomy, University of Geneva, Chemin Pegasi 51, 1290 Versoix, Switzerland
[212]Centro de Astrofísica e Gravitação, Departamento de Física, Instituto Superior Técnico-IST, Universidade de Lisboa-UL, Av. Rovisco Pais 1, 1049-001 Lisboa, Portugal
[213]Eötvös University, Budapest 1117, Hungary
[214]Department of Physical Sciences, Aoyama Gakuin University, 5-10-1 Fuchinobe, Sagamihara City, Kanagawa 252-5258, Japan
[215]University of Sannio at Benevento, I-82100 Benevento, Italy and INFN, Sezione di Napoli, I-80100 Napoli, Italy
[216]California State University, Los Angeles, Los Angeles, California 90032, USA
[217]Instituto de Fisica Teorica UAM-CSIC, Universidad Autonoma de Madrid, 28049 Madrid, Spain
[218]Istituto Nazionale di Astrofisica-Osservatorio di Roma, Viale del Parco Mellini 84–00136 Roma, Italy
[219]Laboratoire d'Acoustique de l'Université du Mans, UMR CNRS 6613, F-72085 Le Mans, France
[220]University of Southampton, Southampton SO17 1BJ, United Kingdom
[221]KAGRA Observatory, Institute for Cosmic Ray Research, The University of Tokyo, 5-1-5 Kashiwa-no-Ha, Kashiwa City, Chiba 277-8582, Japan
[222]Faculty of Physics, University of Białystok, 15-245 Białystok, Poland
[223]University of Nottingham NG7 2RD, United Kingdom
[224]Dipartimento di Ingegneria Industriale, Elettronica e Meccanica, Università degli Studi Roma Tre, I-00146 Roma, Italy
[225]University of Nevada, Las Vegas, Las Vegas, Nevada 89154, USA
[226]University of Chicago, Chicago, Illinois 60637, USA
[227]The University of Mississippi, University, Mississippi 38677, USA
[228]Institute of Physics, Academia Sinica, 128 Sec. II, Academia Rd., Nankang, Taipei 11529, Taiwan
[229]Shanghai Astronomical Observatory, Chinese Academy of Sciences, 80 Nandan Road, Shanghai 200030, China
[230]The Chinese University of Hong Kong, Shatin, NT, Hong Kong
[231]Nirula Institute of Technology, Kolkata, West Bengal 700109, India
[232]American University, Washington, DC 20016, USA
[233]Aix Marseille Université, Jardin du Pharo, 58 Boulevard Charles Livon, 13007 Marseille, France

[234]*Dipartimento di Fisica, Università degli studi di Milano, Via Celoria 16, I-20133, Milano, Italy*
[235]*INFN, sezione di Milano, Via Celoria 16, I-20133, Milano, Italy*
[236]*Department of Applied Physics, Fukuoka University, 8-19-1 Nanakuma, Jonan, Fukuoka City, Fukuoka 814-0180, Japan*
[237]*University of Cambridge, Cambridge CB2 1TN, United Kingdom*
[238]*University of Lancaster, Lancaster LA1 4YW, United Kingdom*
[239]*College of Industrial Technology, Nihon University, 1-2-1 Izumi, Narashino City, Chiba 275-8575, Japan*
[240]*Saha Institute of Nuclear Physics, Bidhannagar, West Bengal 700064, India*
[241]*Institute of Photonics Technologies, National Tsing Hua University, No. 101 Section II, Kuang-Fu Road, Hsinchu 30013, Taiwan*
[242]*Department of Physics, Tamkang University, No. 151, Yingzhuan Rd., Danshui Dist., New Taipei City 25137, Taiwan*
[243]*Department of Electrophysics, National Yang Ming Chiao Tung University, 101 Univ. Street, Hsinchu, Taiwan*
[244]*Rutherford Appleton Laboratory, Didcot OX11 0DE, United Kingdom*
[245]*Department of Astronomy and Space Science, Chungnam National University, 9 Daehak-ro, Yuseong-gu, Daejeon 34134, Republic of Korea*
[246]*Graduate School of Science, Institute of Science Tokyo, 2-12-1 Ookayama, Meguro-ku, Tokyo 152-8551, Japan*
[247]*Columbia University, New York, New York 10027, USA*
[248]*Helmut Schmidt University, D-22043 Hamburg, Germany*
[249]*Nambu Yoichiro Institute of Theoretical and Experimental Physics (NITEP), Osaka Metropolitan University, 3-3-138 Sugimoto-cho, Sumiyoshi-ku, Osaka City, Osaka 558-8585, Japan*
[250]*Directorate of Construction, Services & Estate Management, Mumbai 400094, India*
[251]*Royal Observatory of Belgium, Avenue Circulaire, 3, 1180 Uccle, Belgium*
[252]*Observatoire Astronomique de Strasbourg, Université de Strasbourg, CNRS, 11 rue de l'Université, 67000 Strasbourg, France*
[253]*National Astronomical Observatories, Chinese Academy of Sciences, 20A Datun Road, Chaoyang District, Beijing, China*
[254]*School of Astronomy and Space Science, University of Chinese Academy of Sciences, 20A Datun Road, Chaoyang District, Beijing, China*
[255]*Sungkyunkwan University, Seoul 03063, Republic of Korea*
[256]*Department of Physics, Ulsan National Institute of Science and Technology (UNIST), 50 UNIST-gil, Ulju-gun, Ulsan 44919, Republic of Korea*
[257]*Chung-Ang University, Seoul 06974, Republic of Korea*
[258]*Vrije Universiteit Amsterdam, 1081 HV, Amsterdam, Netherlands*
[259]*University of Washington Bothell, Bothell, Washington 98011, USA*
[260]*Université Paris-Saclay, Université Paris Cité, CEA, CNRS, AIM, 91191, Gif-sur-Yvette, France*
[261]*Ewha Womans University, Seoul 03760, Republic of Korea*
[262]*Department of Astronomy, Yonsei University, 50 Yonsei-Ro, Seodaemun-Gu, Seoul 03722, Republic of Korea*
[263]*National Institute for Mathematical Sciences, Daejeon 34047, Republic of Korea*
[264]*Korea Astronomy and Space Science Institute, Daejeon 34055, Republic of Korea*
[265]*Division of Science, National Astronomical Observatory of Japan, 2-21-1 Osawa, Mitaka City, Tokyo 181-8588, Japan*
[266]*Department of Physics, Aristotle University of Thessaloniki, 54124 Thessaloniki, Greece*
[267]*National Tsing Hua University, Hsinchu City 30013, Taiwan*
[268]*Technical University of Braunschweig, D-38106 Braunschweig, Germany*
[269]*Institute of Mathematics, Polish Academy of Sciences, 00656 Warsaw, Poland*
[270]*Astronomical Observatory, Jagiellonian University, 31-007 Cracow, Poland*
[271]*Department of Physics and Helsinki Institute of Physics, University of Helsinki, Gustaf Hallstromin katu 2, FI-00014, Finland*
[272]*Department of Physics, Nagoya University, ES building, Furocho, Chikusa-ku, Nagoya, Aichi 464-8602, Japan*
[273]*Centre de Calcul IN2P3, 21 avenue Pierre de Coubertin, Campus de la Doua, 69100 Villeurbanne, France*

[274]Université de Montréal/Polytechnique, Montreal, Quebec H3T 1J4, Canada
[275]Università degli Studi di Cagliari, Via Università 40, 09124 Cagliari, Italy
[276]Department of Computer Simulation, Inje University,
197 Inje-ro, Gimhae, Gyeongsangnam-do 50834, Republic of Korea
[277]Korea Astronomy and Space Science Institute (KASI), 776 Daedeokdae-ro, Yuseong-gu, Daejeon 34055, Republic of Korea
[278]NAVIER, École des Ponts, Univ Gustave Eiffel, CNRS, Marne-la-Vallée, France
[279]Gravitational Wave Science Project, National Astronomical Observatory of Japan (NAOJ), Mitaka City, Tokyo 181-8588, Japan
[280]Department of Physics, National Cheng Kung University,
No.1, University Road, Tainan City 701, Taiwan
[281]National Center for High-performance Computing, National Institutes of Applied Research, No. 7, R&D 6th Rd., Hsinchu Science Park, Hsinchu City 30076, Taiwan
[282]Institute of Astronomy, National Tsing Hua University,
No. 101 Section II, Kuang-Fu Road, Hsinchu 30013, Taiwan
[283]Institució Catalana de Recerca i Estudis Avançats, E-08010 Barcelona, Spain
[284]Institut fuer Theoretische Astrophysik, Zentrum fuer Astronomie Heidelberg, Universitaet Heidelberg, Albert Ueberle Str. 2, 69120 Heidelberg, Germany
[285]Institucio Catalana de Recerca i Estudis Avançats (ICREA),
Passeig de Lluís Companys, 23, 08010 Barcelona, Spain
[286]Université de Lyon, Université Claude Bernard Lyon 1, CNRS,
Institut Lumière Matière, F-69622 Villeurbanne, France
[287]Universidade Estadual Paulista, R. Dr. José Barbosa de Barros, 1780-Jardim Paraiso, Botucatu-SP, 18610-307, Brazil
[288]Tsinghua University, Beijing 100084, China
[289]Departament de Física, Universitat de les Illes Balears, IAC3—IEEC, Crta. Valldemossa km 7.5, E-07122 Palma, Spain
[290]Universidad de Guadalajara, 44430 Guadalajara, Jalisco, Mexico
[291]Institut des Hautes Etudes Scientifiques, F-91440 Bures-sur-Yvette, France
[292]Faculty of Law, Ryukoku University, 67 Fukakusa Tsukamoto-cho,
Fushimi-ku, Kyoto City, Kyoto 612-8577, Japan
[293]Indian Institute of Science Education and Research, Kolkata, Mohanpur, West Bengal 741252, India
[294]Phenikaa University, Nguyen Trac Street, Duong Noi, Hanoi, Vietnam
[295]University of Stavanger, 4021 Stavanger, Norway
[296]Department of Astronomy, The University of Tokyo, 7-3-1 Hongo, Bunkyo-ku, Tokyo 113-0033, Japan
[297]Physics Program, Graduate School of Advanced Science and Engineering, Hiroshima University, 1-3-1 Kagamiyama, Higashihiroshima City, Hiroshima 739-8526, Japan
[298]GRAPPA, Anton Pannekoek Institute for Astronomy and Institute for High-Energy Physics, University of Amsterdam, 1098 XH Amsterdam, Netherlands
[299]University College London, London WC1E 6BT, United Kingdom
[300]Observatoire de Paris, 75014 Paris, France
[301]Instituto Tecnológico de Aeronáutica, Praça Marechal Eduardo Gomes, 50-Vila das Acacias, São José dos Campos-SP, 12228-900, Brazil
[302]Graduate School of Science and Technology, Niigata University, 8050 Ikarashi-2-no-cho, Nishi-ku, Niigata City, Niigata 950-2181, Japan
[303]Niigata Study Center, The Open University of Japan, 754 Ichibancho, Asahimachi-dori, Chuo-ku, Niigata City, Niigata 951-8122, Japan
[304]Consiglio Nazionale delle Ricerche-Istituto dei Sistemi Complessi, I-00185 Roma, Italy
[305]Hobart and William Smith Colleges, Geneva, New York 14456, USA
[306]Dipartimento di Ingegneria, Università del Sannio, I-82100 Benevento, Italy
[307]Institut d'Astrophysique de Paris, Sorbonne Université, CNRS, UMR 7095, 75014 Paris, France
[308]Museo Storico della Fisica e Centro Studi e Ricerche "Enrico Fermi," I-00184 Roma, Italy
[309]Kennesaw State University, Kennesaw, Georgia 30144, USA
[310]Government Victoria College, Palakkad, Kerala 678001, India
[311]Universidad de Antioquia, Medellín, Colombia
[312]Departamento de Física-ETSIDI, Universidad Politécnica de Madrid, 28012 Madrid, Spain
[313]Ariel University, Ramat HaGolan St 65, Ariel, Israel

[314]*Department of Electronic Control Engineering, National Institute of Technology, Nagaoka College, 888 Nishikatakai, Nagaoka City, Niigata 940-8532, Japan*
[315]*Dipartimento di Fisica e Scienze della Terra, Università Degli Studi di Ferrara, Via Saragat, 1, 44121 Ferrara FE, Italy*
[316]*Faculty of Science, Toho University, 2-2-1 Miyama, Funabashi City, Chiba 274-8510, Japan*
[317]*Seoul National University, Seoul 08826, Republic of Korea*
[318]*Kavli Institute for Astronomy and Astrophysics, Peking University, Yiheyuan Road 5, Haidian District, Beijing 100871, China*
[319]*Faculty of Information Science and Technology, Osaka Institute of Technology, 1-79-1 Kitayama, Hirakata City, Osaka 573-0196, Japan*
[320]*NASA Goddard Space Flight Center, Greenbelt, Maryland 20771, USA*
[321]*Faculty of Science and Technology, Kochi University, 2-5-1 Akebono-cho, Kochi-shi, Kochi 780-8520, Japan*
[322]*Concordia University Wisconsin, Mequon, Wisconsin 53097, USA*
[323]*Scuola Internazionale Superiore di Studi Avanzati, Via Bonomea, 265, I-34136, Trieste TS, Italy*
[324]*Laboratoire de Physique de l'ENS, Université Paris Cité, Ecole Normale Supérieure, Université PSL, Sorbonne Université, CNRS, 75005 Paris, France*
[325]*Universidade Estadual Paulista, 01140-070 São Paulo, Brazil*
[326]*The Hakubi Center for Advanced Research, Kyoto University, Yoshida-honmachi, Sakyou-ku, Kyoto City, Kyoto 606-8501, Japan*
[327]*Department of Physics, Kyoto University, Kita-Shirakawa Oiwake-cho, Sakyou-ku, Kyoto City, Kyoto 606-8502, Japan*
[328]*Yukawa Institute for Theoretical Physics (YITP), Kyoto University, Kita-Shirakawa Oiwake-cho, Sakyou-ku, Kyoto City, Kyoto 606-8502, Japan*
[329]*University of Catania, Department of Physics and Astronomy, Via S. Sofia, 64, 95123 Catania CT, Italy*
[330]*Southeastern Louisiana University, Hammond, Louisiana 70402, USA*
[331]*National Institute of Technology, Fukui College, Geshi-cho, Sabae-shi, Fukui 916-8507, Japan*
[332]*Department of Communications Engineering, National Defense Academy of Japan, 1-10-20 Hashirimizu, Yokosuka City, Kanagawa 239-8686, Japan*
[333]*Eindhoven University of Technology, 5600 MB Eindhoven, Netherlands*
[334]*School of Physics and Technology, Wuhan University, Bayi Road 299, Wuchang District, Wuhan, Hubei, 430072, China*
[335]*Kavli Institute for the Physics and Mathematics of the Universe (Kavli IPMU), WPI, The University of Tokyo, 5-1-5 Kashiwa-no-Ha, Kashiwa City, Chiba 277-8583, Japan*
[336]*Department of Astronomy, Beijing Normal University, Xinjiekouwai Street 19, Haidian District, Beijing 100875, China*
[337]*Hong Kong University of Science and Technology, Clear Water Bay, HK, Hong Kong*

[a]Deceased March 2026.
[b]Deceased August 2025.